Modeling Photosynthesis and Exudation of DOM in Subtropical Oceans

Zhen Wu[1], Stephanie Dutkiewicz[1], Oliver Jahn[1], Daniel Sher[2], Angelicque White[3], Michael J. Follows[1]

[1]Department of Earth, Atmospheric and Planetary Sciences, Massachusetts Institute of Technology, Cambridge, Massachusetts, USA
[2]Department of Marine Biology, Leon H. Charney School of Marine Sciences, University of Haifa, Haifa, Israel
[3]Department of Oceanography, University of Hawaii at Manoa, Honolulu, Hawaii, USA

Key Points:

- Decoupling of photosynthesis and biosynthesis improved simulations of primary production
- Predicted global primary production increased by 35%
- Model results suggest exudation could contribute $\sim$ 20% to total DOC source in euphotic layer

Corresponding author: Zhen Wu, zhenwu@mit.edu

Abstract

Parameterizations of algal photosynthesis commonly employed in global biogeochemical simulations generally fail to capture the observed vertical structure of primary production. Here we examined the consequences of decoupling photosynthesis (carbon fixation) and biosynthesis (biomass building) with accumulation or exudation of excess photosynthate under energy rich conditions in both regional and global models. The results show that the decoupling of these two processes improved the simulated vertical profile of primary production, increased modeled global primary production up to $\sim 35\%$, improved simulated meridional patterns of particulate C:N:P and increased modeled surface pool of semi-labile DOC.

1 Introduction

The structure and rates of photosynthesis and biosynthesis by primary producers in the ocean's subtropical gyres reflect the balance between photons delivered from above, macronutrients delivered largely from below, and essential trace metals such as iron which has both oceanic and atmospheric sources. The observed vertical profiles in Fig.1 from North Pacific and North Atlantic subtropical gyres (Karl & Church, 2014; White et al., 2015; Steinberg et al., 2001; Letelier et al., 1996) reveal the transition from nutrient to light limitation over a relatively short distance (less than 100m). Primary production is often highest at the surface, decreasing with depth (Fig.1) while Chlorophyll-a concentrations (Chla) are elevated in a region termed the Deep Chlorophyll Maximum (DCM), characterized by persistent light limitation and proximity to the nitracline (Letelier et al., 2004). In contrast, particulate organic carbon (POC; including living biomass) is more uniform over the upper 75 m leading to a vertical gradient in mass normalized primary production. These vertical contrasts suggest a decoupling of photosynthesis (the fixation of CO_2 into carbohydrates) and biosynthesis (production of a suite of functional macromolecules including proteins) over the light gradient. Yet commonly employed biogeochemical models treat photosynthesis and biosynthesis as tightly coupled processes limited by light, temperature, and nutrients (e.g. Dutkiewicz et al. (2015); Dunne et al. (2013); Aumont et al. (2015)). These models typically represent the carbon-specific photosynthesis rate for phytoplankton type j, $P_{C,j}$ ($mmol\ C\ (mmol\ C)^{-1}\ d^{-1}$), as a function of irradiance, and a flexible Chla:C ratio following Geider et al. (1997):

$$P_{C,j} = P_{C,j}^{Sat}\left[1 - exp\left(-\frac{\alpha I\ \theta_j}{P_{C,j}^{Sat}}\right)\right] \tag{1}$$

where, α is the initial slope of the photosynthesis-irradiance curve normalized to Chla ($m^2\ (mg\ Chla)^{-1}\ mmol\ C\ (\mu mol\ photons)^{-1}$), I is the flux of photosynthetically active radiation (PAR, $\mu mol\ photons\ m^{-2}\ s^{-1}$), θ_j is the Chla:C ratio of phytoplankton type j ($mg\ Chla\ (mmol\ C)^{-1}$). The light-saturated photosynthetic rate for type j, $P_{C,j}^{Sat}$ ($mmol\ C\ (mmol\ C)^{-1}\ d^{-1}$), is typically modeled as dependent on both temperature and nutrient availability:

$$P_{C,j}^{Sat} = P_{C,j}^{max}\frac{Nut}{Nut + K_{Nut,j}} \cdot T_{func} \tag{2}$$

Following Geider et al. (1997), temperature dependence is introduced through a multiplicative function T_{func} (e.g. Arrhenius equation), and there is an explicit accounting of nutrient limitation through a multiplicative, hyperbolic function of Nut, the limiting nutrient concentration. The latter throttles back photosynthesis in low nutrient environments with the consequence of tightly coupling photosynthesis and biosynthesis. However, the two processes may not be so tightly coupled. For example, photosynthesis can be limited by the availability of light or photosynthetic apparatus (Mackey et al., 2008; Letelier et al., 2017), while biosynthesis is limited by the cellular reserves and external availability of nitrogen (N), phosphorus (P), or iron (Fe) (Marañón et al., 2013; Halsey & Jones, 2015) as well as the necessary self-replicating apparatus.

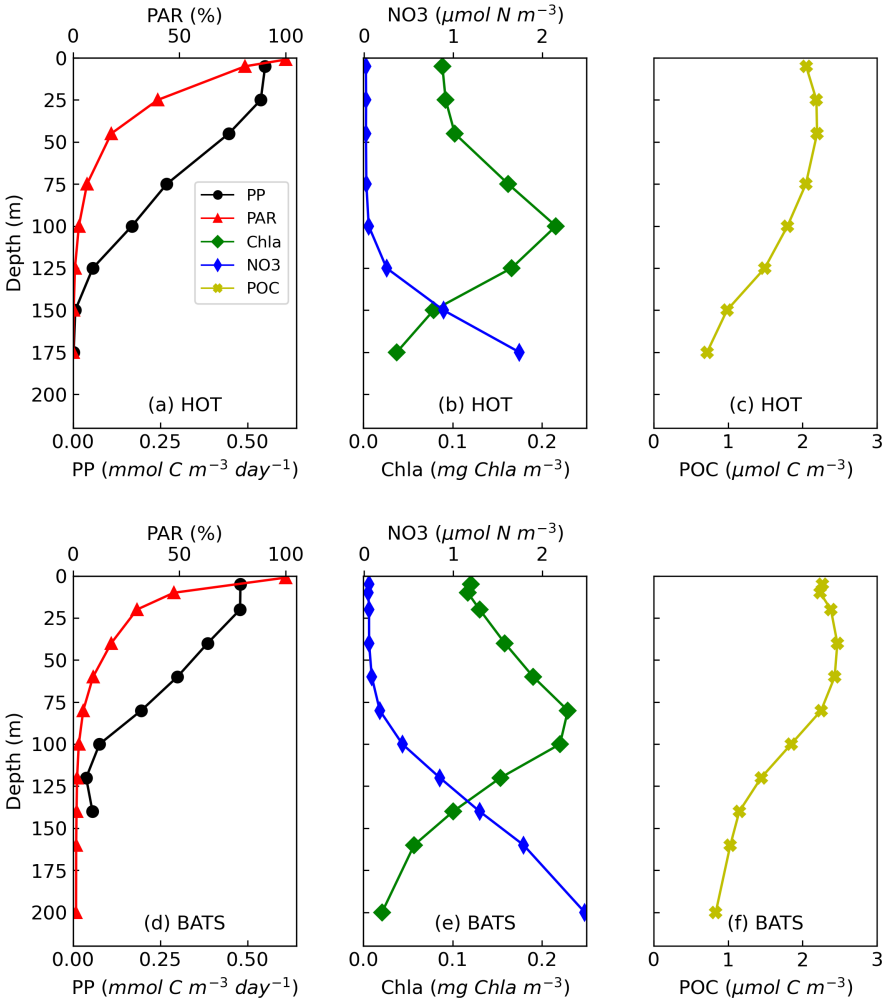

Figure 1. Observed climatological average of photosynthesis rate, Chla, nitrate, particulate organic carbon (POC), and photosynthetically active radiation (PAR) at HOT and BATS. The data were obtained from the observations from 1988 to 2018 at both stations.

Phytoplankton may balance the supply and demand of photosynthesis and biosynthesis by the regulation of nutrient uptake (Flynn, 2003), "luxury storage" of resources in excess of demand (Martin et al., 2014) or the exudation of excess photosynthate (Halsey & Jones, 2015). The excretion of DOM in nutrient replete, exponentially growing cultures phytoplankton is low, $\sim$ 2% of total gross carbon fixation (López-Sandoval et al., 2013). However, recent studies show that *Prochlorococcus*, an abundant pico-cyanobacterium found in oligotrophic ocean regions and which only have a moderate ability for photoacclimation, can excrete a large fraction of fixed C under nutrient-limited conditions (Thompson et al., 2018; Cailliau et al., 1996; Szul et al., 2019; Kulk et al., 2011; Bertlisson et al., 2005; Roth-Rosenberg et al., 2021). Thus exudation is more likely significant in the oligotrophic surface ocean where there is persistent nutrient limitation and light-saturating conditions. The exudates may be a source of carbon for heterotrophic bacteria (Berman & Holm-Hansen, 1974; Bjørrisen, 1988), which increase remineralization and total ecosystem biomass, hence promoting the co-evolution of phototrophic and heterotrophic populations (Braakman et al., 2017; Sarmento et al., 2016).

Here we use numerical models to investigate the consequences of decoupling photosynthesis and biosynthesis on the simulation of primary production in the oligotrophic gyres, as well as the global rates of photosynthesis and potential exudation of DOC. First, we briefly describe the 1D and 3D models with particular emphasis on the treatment of photosynthesis and its coupling to biosynthesis (Methods, 2). We demonstrate, using a high vertical-resolution, 1D model that the "standard" photosynthesis parameterization does not capture the observed vertical profile of primary production. In particular, it strongly underpredicts photosynthesis in the nutrient depleted surface layer. We find that removing direct macronutrient limitation on photosynthesis, but retaining the indirect cost of maintaining photosynthetic machinery, significantly improves the vertical structure and vertically integrated rates of primary production in 1D water column simulations. It also increases global primary production and DOC production by about 30% in a 3D global model (See Section 3).

2 Methods

2.1 Environmental Modeling Framework

The biogeochemical-ecosystem model describes the cycling of carbon, nitrogen, phosphorus, iron, silica and oxygen in both living and non-living forms as discussed in Follows et al. (2007) and Dutkiewicz et al. (2015). We employ one-dimensional (1D) and three-dimensional (3D) physical configurations with identical biogeochemistry and ecology. We first examine the qualitative impact of decoupling carbon and nutrient flows in vertically well-resolved 1D simulations and then quantitatively evaluate the impact in 3D global simulations.

The 1D simulations were configured to resolve only the vertical dimension in space. The 6000 m deep column has a vertical resolution of 10 m from sea surface to 120 m depth and with gradually increasing thickness thereafter. Nutrient distributions and plankton biomass were initialized according to World Ocean Atlas (Garcia et al., 2018) and previous 3D simulations relevant to HOT (Hawaii Ocean Time-series) in the North Pacific Subtropical Gyre and BATS (Bermuda Atlantic Time-Series) in the North Atlantic (Dutkiewicz et al., 2015). In this configuration, a seasonal mixed layer was driven by restoring to climatological, seasonal sea surface temperatures which drives winter-time convection following Hickman et al. (2010). The 1D framework does not resolve the contributions of isopycnal nutrient transport nor the effect of mesoscale motions, tides, and internal waves which drive intermittent nutrient transfer into the euphotic zone (McGillicuddy, 2016). Hence, the vertical, diapycnal diffusivity for HOT and BATS were modified to parameterize these processes. The time step of 1D configuration is 1h and we integrate the 1D configuration for 30 years with a repeating generic "year" of external forcings. The model results establish a repeating pattern after several years spin-up leading to a "quasi-steady state" by year 10. In the analysis presented below we consider the climatology of the last 15 years of 30 year simulations.

The 3D configuration of the MIT general circulation model (MITgcm) (Marshall et al., 1997) has a horizontal resolution of $1^\circ \times 1^\circ$. There are 23 vertical levels, 10m for the top two levels, and then graduated in thickness to 500m at depth. The physical fields are constrained by satellite and in-situ observations (Wunsch & Heimbach, 2007) (the ECCO-GODAE state estimate), which is used by many previous biogeochemical-ecosystem studies (Follows et al., 2007; Ward et al., 2012; Dutkiewicz et al., 2015; Ward & Follows, 2016). The 3D simulations were initialized by World Ocean Atlas (Garcia et al., 2018) for nitrate, phosphate, and silicic acid and previous model output for iron, ammonium, nitrite, dissolved and particulate matter, and plankton biomass. We integrate the system forward in time for 10 years from initial conditions provided by an earlier simulation. The simulated phytoplankton establish a repeating pattern after about 4 years after which the system represents a "quasi-steady

state" with a slow, longer term adjustment in nutrient fields not affecting the results that we discuss here. We show results from the tenth year of the simulation.

We resolve two size classes of phytoplankton (picophytoplankton and all others) as well as two types of grazers. The biogeochemical and biological tracers interact through the formation, transformation, and remineralization of organic matter. Mortality, sloppy feeding, and exudation transfer living organic material into sinking particulate and dissolved organic detritus which are respired back to inorganic form with simple parameterizations of the activity of heterotrophic decomposers. Iron cycling includes scavenging by particles and explicit complexation with an organic ligand following Dutkiewicz et al. (2015). Aeolian iron fluxes to the ocean surface are provided by Luo et al. (2008). The complete model equations and descriptions are provided in the Supporting Information.

2.2 Cellular Stoichiometry and Photosynthesis

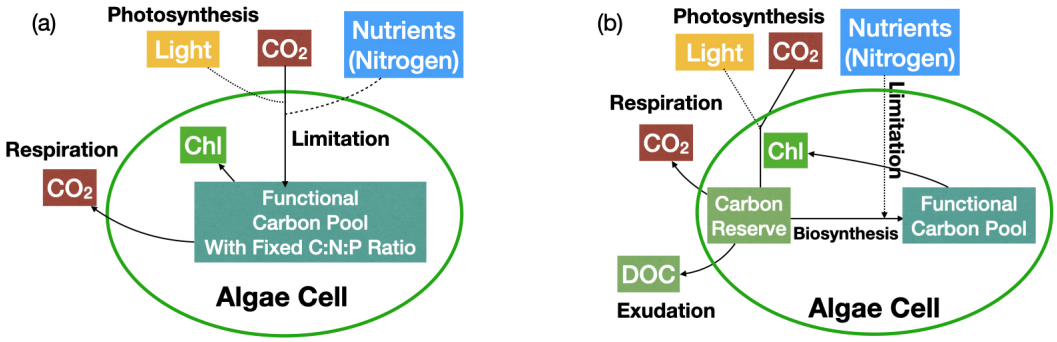

Figure 2. Schematic representations of cellular C flow. (a) represents the model in which C and N flow are tightly coupled. (b) represents the model in which C and N flow are decoupled.

In this study, we examine the biogeochemical implications of decoupling carbon and nutrient flow by comparing two physiological parameterizations (see Fig.2). In the "standard model" (depicted in Fig.2a) following Eq.2 (Geider et al., 1997), photosynthesis is directly influenced by the external concentration of fixed nitrogen (proportional to $[NO_3^-]/([NO_3^-]+K_{NO_3})$). In the "decoupled model", (depicted in Fig.2b) carbon and nitrogen flows are buffered by independent reserves (following, for example, Talmy et al. (2014), Bruggeman and Kooijman (2007)) and the light-saturated photosynthesis rate is not directly dependent on the external fixed-nitrogen availability (compare to Eq.2):

$$P_{C,j}^{Sat} = P_{C,j}^{max} \cdot T_{func} \tag{3}$$

Here photosynthesis is sensitive to nitrogen availability only indirectly through Chla which is controlled by the rate of biosynthesis. Biosynthesis is controlled by the availability of reserves of both photosynthate and other nutrient elements. In the decoupled model, the rate of photosynthesis continues to be controlled by the light environment even when biosynthesis is nitrogen limited. In that case, excess photosynthate is stored in the reserve or exuded. The mathematical details of these parameterizations are described below.

2.3 Details of physiological parameterizations.

In Eq.1 and Eq.2, $P_{C,j}^{max}$ is the maximum carbon-normalized photosynthesis rate of phytoplankton j $(mmol\ C\ (mmol\ C)^{-1}\ d^{-1})$, T_{func} represents the temperature limitation

Table 1. Biological parameters of different phytoplankton functional types.

Parameter	Symbol	Type I	Type II	Unit
Maximum photosynthesis rate	P_C^{max}	0.76	3.15	$mmol\ C\ (mmol\ C)^{-1}\ d^{-1}$
Maximum uptake rate	$V_{NO_3}^{max}$	0.49	0.14	$mmol\ N\ (mmol\ C)^{-1}\ d^{-1}$
	$V_{NO_2}^{max}$	0.49	0.14	$mmol\ N\ (mmol\ C)^{-1}\ d^{-1}$
	$V_{NH_4}^{max}$	0.24	0.07	$mmol\ N\ (mmol\ C)^{-1}\ d^{-1}$
	$V_{PO_4}^{max}$	0.014	0.01	$mmol\ P\ (mmol\ C)^{-1}\ d^{-1}$
	V_{Fe}^{max}	1.83×10^{-5}	9.92×10^{-6}	$mmol\ Fe\ (mmol\ C)^{-1}\ d^{-1}$
Half-saturation concentration	K_{NO_3}	2.76×10^{-3}	0.41	$mmol\ N\ m^{-3}$
	K_{NO_2}	2.76×10^{-3}	0.41	$mmol\ N\ m^{-3}$
	K_{NH_4}	1.38×10^{-3}	0.21	$mmol\ N\ m^{-3}$
	K_{PO_4}	1.73×10^{-4}	0.026	$mmol\ P\ m^{-3}$
	K_{FeT}	1.73×10^{-7}	2.59×10^{-5}	$mmol\ Fe\ m^{-3}$
Celluar stoichiometric ratios	$R_{C:N}$	7.5	7.5	$mmol\ C\ (mmol\ N)^{-1}$
	$R_{C:P}$	120.0	120.0	$mmol\ C\ (mmol\ P)^{-1}$
	$R_{C:Fe}$	1.2×10^5	1.2×10^5	$mmol\ C\ (mmol\ Fe)^{-1}$

on photosynthesis:

$$T_{func} = \tau \cdot exp\left[A_E\left(\frac{1}{T + 273.15} - \frac{1}{T_0}\right)\right] \tag{4}$$

where τ is Arrhenius coefficient, A_E is the slope of the linear region of the Arrhenius plot, T_0 is the reference temperature of phytoplankton j (K), and T is water column temperature ($^\circ C$).

Photosynthate is delivered to a "reserve" (carbohydrate or lipid) from where it may be used for biosynthesis or exuded. The potential rates of uptake of nutrients other than carbon (nitrogen, phosphorus, iron) are evaluated with Michaelis-Menten kinetics and an Arrhenius temperature dependence, following Eq.5 and Eq.6.

$$V_{R,j} = V_{R,j}^{max} \cdot \gamma_{R,j} \cdot T_{func} \tag{5}$$

$$\gamma_{R,j} = \frac{R}{R + K_{R,j}} \tag{6}$$

where $V_{R,j}^{max}$ is the maximum carbon-normalized uptake rate for resource R of phytoplankton j ($mmol\ R\ (mmol\ C)^{-1}\ d^{-1}$), $\gamma_{R,j}$ is the nutrient limitation based on Michaelis-Menten kinetics, $K_{R,j}$ is the half-saturation concentration of resource R of phytoplankton j ($mmol\ R\ m^{-3}$). The total potential uptake of nitrogen is defined as the sum of the uptake of each species in Eq.7.

$$V_{N,j} = V_{NH_4,j} + V_{NO_3,j} + V_{NO_2,j} \tag{7}$$

The carbon demand to build biomass, $D_{i,j}$ ($mmol\ C\ (mmol\ C)^{-1}\ d^{-1}$), for each nutrient element i and each phytoplankton type j, is evaluated based on an assumed, fixed stoichiometry of functional biomass (e.g. protein, nucleic acids, etc) in Eq.8.

$$D_{i,j} = V_{i,j} \cdot R_j^{C:i} \tag{8}$$

where i denotes N, P, Fe, $R_j^{C:i}$ is the $C:i$ ratio in phytoplankton j ($mmol\ C\ (mmol\ i)^{-1}$). The carbon-specific production of functional biomass (biosynthesis) is then determined as

the minimum of the photosynthesis rate and the carbon demand of the most limiting nutrient in Eq.9 and Eq.10.

$$BS_{C,j} = min[D_{min,j}, P_{C,j}] \tag{9}$$

$$D_{min,j} = min[D_{N,j}, D_{P,j}, D_{Fe,j}] \tag{10}$$

Previously published models of exudation in laboratory cultures (Grossowicz, Roth-Rosenberg, et al., 2017; Grossowicz, Marques, & van Voorn, 2017; Vallino, 2000; Flynn et al., 2008) have parameterized exudation as a simple, imposed fraction of primary production or with more complex approaches linked to nutrient limitation, biomass, and nutrient stoichiometry (see the review of Livanou et al. (2019)). Here we assume that if the photosynthesis rate is greater than growth rate (which means biosynthesis is limited by nutrients rather than light energy), a fraction of the excess photosynthate accumulates in the carbon reserve and the remainder $f_{e,j}$ is assumed exuded into the environment at the rate of $E_{C,j}$ ($mmol\ C\ (mmol\ C)^{-1}\ d^{-1}$) as described in Eq.11. In the results we assume $f_{e,j}$=0.7 in Fig.4-6 . We examine this choice later in this manuscript.

$$E_{C,j} = max[0.0, P_{C,j} - BS_{C,j}] \cdot f_{e,j} \tag{11}$$

We parameterize the two classes of phytoplankton as pico-phytoplankton (type I) with high nutrient affinity, but low growth rates, and the larger phytoplankton (type II) with lower nutrient affinity and higher growth (Follows et al., 2007). Values of the parameters (Table 1) are similar to the cyanobacteria and diatom values used in Dutkiewicz et al. (2020).

3 Results and Discussion.

First we examine the qualitative impact of decoupling carbon and nutrient flows on the vertical structure of modeled primary production in a 1D framework, referencing observed profiles at HOT and BATS. Then we examine the quantitative impact on integrated primary production in 3D global simulations. For this discussion, we will refer to the simulations in which N and C flow are tightly coupled as the "standard" simulations and those in which N and C flow are decoupled as the "decoupled" simulations.

3.1 Vertical Profiles of Subtropical Productivity

We first examine qualitative differences between 1D simulations where photosynthesis is explicitly limited by nutrient concentrations following Eq.2 ("standard" model, Fig.2a) to simulations where photosynthesis depends on nutrients only indirectly through the rate of biosynthesis for photosynthetic pigments ("decoupled" model, Fig.2b, also see Eq.S20-21 in Supporting Information). The climatologies of the last 15 years of the simulations are compared with climatological data from HOT (1988-2018) and BATS (1989-2016). Some general features of the two sites were qualitatively captured in both simulations (Fig.3) including the late winter bloom at BATS and the DCM at both sites (during the summer at BATS and year-round at HOT). As observed, simulated seasonality at HOT was much weaker than at BATS due to the difference in seasonal physical forcing (Malmstrom et al., 2010; Karl & Church, 2014; Steinberg et al., 2001; Cavender-Bares et al., 2001).

However, the standard and decoupled simulations also show some significant differences with one-another which we highlight in Fig.4. Due to the explicit throttling back of photosynthesis in the highly oligotrophic surface waters caused by nutrient limitation, the standard model fails to capture the increase of photosynthesis towards the surface both at HOT and, more strikingly, at BATS. The standard model consistently predicts extremely low photosynthesis rates near the surface relative to the observed climatologies. In contrast, the solid blue lines in Fig.4 indicate the simulations of the decoupled model. Here photosynthesis was not throttled back under low nitrogen conditions however nitrogen lim-

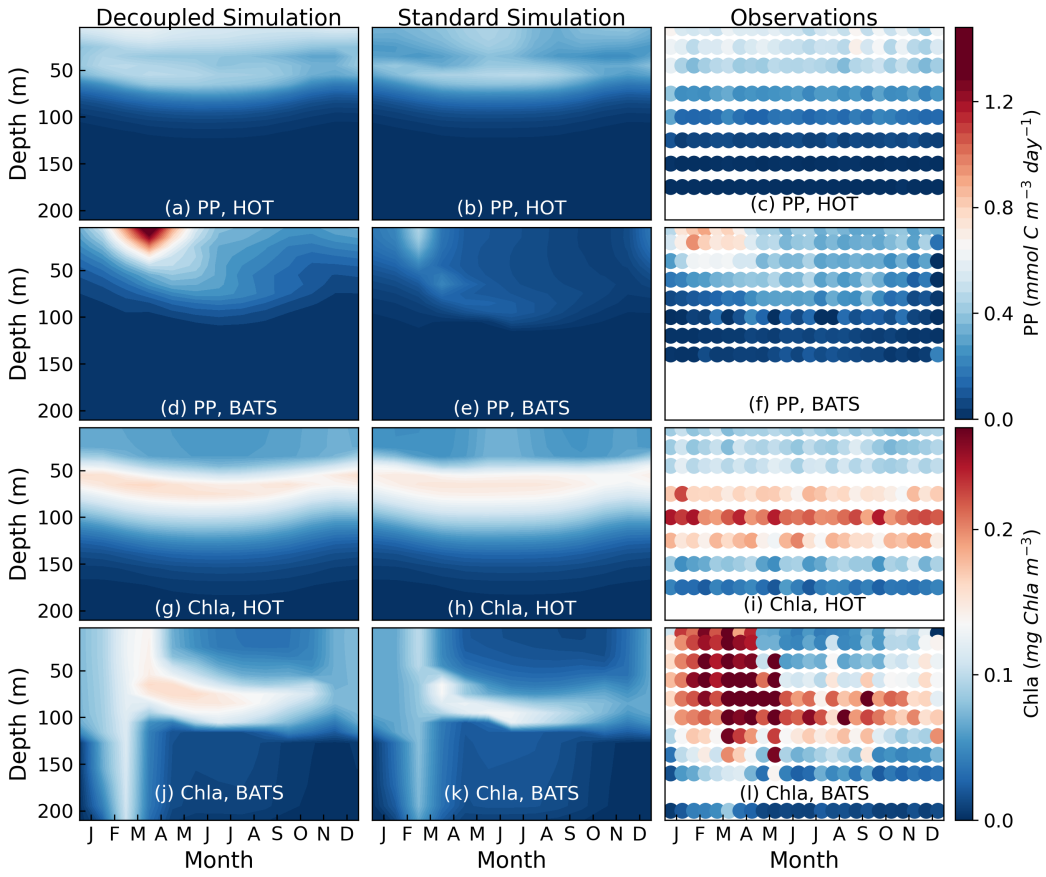

Figure 3. One-dimensional model simulations: seasonal variation and biases of photosynthesis rate and Chla at HOT and BATS. (a) photosynthesis rate of decoupled simulation at station ALOHA ($mmol\ C\ m^{-3}\ d^{-1}$); (b) photosynthesis rate of standard simulation at station ALOHA ($mmol\ C\ m^{-3}\ d^{-1}$); (c) observed photosynthesis rate at station ALOHA ($mmol\ C\ m^{-3}\ d^{-1}$); (d) photosynthesis rate of decoupled simulation at station Bermuda ($mmol\ C\ m^{-3}\ d^{-1}$); (e) photosynthesis rate of standard simulation at station Bermuda ($mmol\ C\ m^{-3}\ d^{-1}$); (f) observed photosynthesis rate at station Bermuda ($mmol\ C\ m^{-3}\ d^{-1}$); (g) Chla concentration of decoupled simulation at station ALOHA ($mg\ Chla\ m^{-3}$); (h) Chla concentration of standard simulation at station ALOHA ($mg\ Chla\ m^{-3}$); (i) observed Chla concentration at station ALOHA ($mg\ Chla\ m^{-3}$); (j) Chla concentration of decoupled simulation at station Bermuda ($mg\ Chla\ m^{-3}$); (k) Chla concentration of standard simulation at station Bermuda ($mg\ Chla\ m^{-3}$); (l) observed Chla concentration at station Bermuda ($mg\ Chla\ m^{-3}$).

itation does control biosynthesis of pigments. The vertical profiles of primary production increase towards the surface, both qualitatively and quantitatively more consistent with the observations.

The vertically integrated rate of photosynthesis (0-200m) in the decoupled experiments is increased by ∼21.1% at HOT and more than 170% at BATS compared to the standard simulation. In the upper 200m of the decoupled simulations, photosynthesis exceeded biosynthesis rate by ∼25% at HOT and ∼58% at BATS. Excess photosynthate in the decoupled simulations accumulates as storage in the cells or is exuded, consistent with numerous laboratory and field studies (Thornton, 2014; Szul et al., 2019; Bjørrisen, 1988). However,

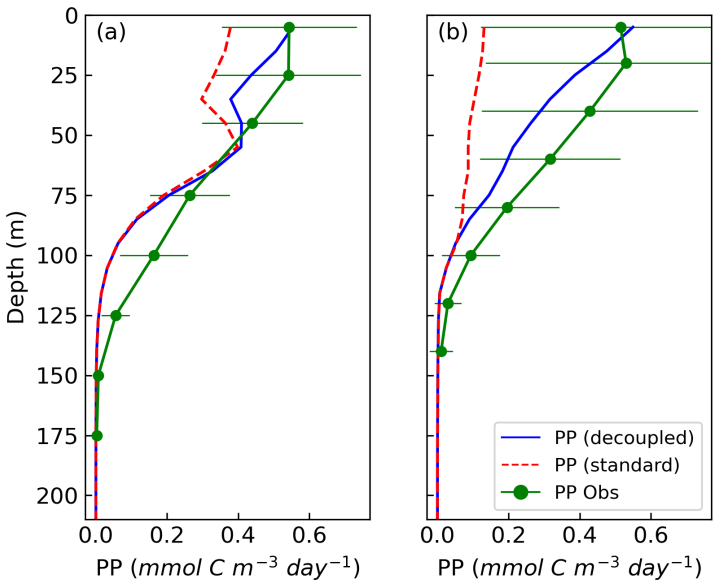

Figure 4. Annual averaged vertical profiles of primary production at (a) HOT and (b) BATS. Model results are annual averages from the last 15 years of 30 year integrations. The green solid lines indicate observed primary production from 1988 to 2016 and the horizontal green bars represent deviation of the inter-annual variations. The red dashed lines indicate the standard simulation, where photosynthesis is directly regulated by local nutrient concentration. The blue solid lines represent simulations of photosynthesis rate in the decoupled simulation.

due to the complexity of DOC composition, we do not address the fate of excess photosynthate in detail in the decoupled simulation, but instead examine the general consequences of the balance between storage and exudation for the C:N:P ratio of phytoplankton biomass and production of DOC in the following 3D study.

3.2 Global Biomass and Productivity

In the previous section we demonstrated that the decoupling of N and C flow in the physiological model leads to a significant qualitative improvement in simulations of the vertical profile of primary production. We now examine the implications for the prediction of global-scale primary productivity and elemental composition of phytoplankton (and particulate matter) by comparing global 3D standard and decoupled simulations.

Both standard and uncoupled simulations capture the high surface Chla, primary production, and nutrient concentrations in the subpolar and equatorial regimes, as well as low surface Chla, primary production, and nutrient concentrations in subtropical gyres (Fig.5, also see Fig.S1). Typical for such coarse resolution simulations, the dynamics and biogeochemistry of continental shelves and coastal regions are not resolved or well represented.

We asked what is the sensitivity of globally integrated primary production to the decoupling of nutrient and C at the cellular scale? Modeled global primary production of the standard and decoupled simulations were 34.0 $Pg\ C \cdot yr^{-1}$ and 45.8 $Pg\ C \cdot yr^{-1}$ respectively - an increase of 34%. Satellite-derived estimates range between $44 - 57\ Pg\ C \cdot yr^{-1}$ with the mean of 50.7 $Pg\ C \cdot yr^{-1}$ (Carr et al., 2006; Field et al., 1998; Silsbe et al., 2016) suggesting that the decoupled estimate is potentially more plausible. However, there are large uncer-

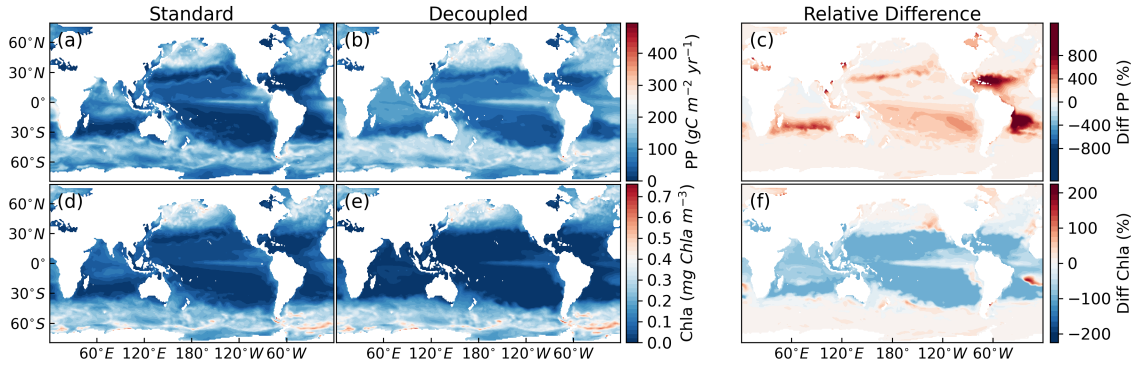

Figure 5. Comparison of standard and decoupled simulations of Chla and primary production(PP). (a) simulated primary production of standard model (0-55 m depth integrated, $gC\ m^{-2}\ yr^{-1}$), (b) simulated primary production of decoupled model (0-55 m depth integrated, $gC\ m^{-2}\ yr^{-1}$), (c) difference of primary production between standard and decoupled simulations (%), (d) simulated Chla of standard model (mean 0-55 m, $mg\ Chla\ m^{-3}$), (e) simulated Chla of decoupled model (mean 0-55 m, $mg\ Chla\ m^{-3}$), (f) difference of Chla between standard and decoupled simulations (%).

tainties underlying in both ocean color based and general circulation model based estimates of global primary production ranging from $\sim 35\ to\ \sim 70\ Pg\ C \cdot yr^{-1}$ (Carr et al., 2006).

The 1D simulations indicated a significant improvement in the simulation of the vertical profile of primary production. We have used a Taylor diagram (Taylor, 2001) to compare the spatial variations of primary production in the two 3D simulations (standard and decoupled) against a suite of remote-sensing derived estimates of global-scale patterns and rates of primary production (Behrenfeld & Falkowski, 1997; Westberry et al., 2008; Silsbe et al., 2016) (Fig.6; also Fig.S2). We focused on open ocean regimes having bottom depths greater than 500 m since the global model does not resolve coastal systems and remote sensing algorithms are typically modified.

A comparison of the decoupled simulation with various remote sensing primary production products revealed similar variability (standard deviation) but a range of poor to weak spatial correlation. However, the correlations of spatial variations between the various remote sensing products themselves was just as broad ranging and also as weak as simulations. The satellite-derived products also have large error margins associated with them that are not spatially homogeneous (Szeto et al., 2011). Thus we could not quantitatively distinguish whether either standard or decoupled simulation has more skill by comparing patterns of primary production.

The difference in primary production between decoupled and standard simulations however mainly lies in oligotrophic gyres where there is a low nutrient nutrient supply rate relative to the incoming light energy, as illustrated in Fig.5. The difference is most notable in the Atlantic subtropical gyres where macro-nutrients were most depleted in the simulations (NO_3 fields showed Fig.S1(a)). The standard simulation of primary production in subtropical gyres is too low relative to all the satellite-based products (Fig.S2). The increased primary production in these regions in the decoupled simulation (Fig.5, Fig.S2) suggests that the decoupling of carbon and nitrogen flow does indeed improve modelled primary production.

The difference in Chla between decoupled and standard simulations is also most pronounced in the oligotrophic subtropical gyres. Chla decreases in the decoupled model relative to the standard model because Chla synthesis is regulated by the ratio of photosynthesis rate and light harvesting rate resulting in a negative relationship with $P^{Sat}_{C,j}$ (see Eq.S20-21 in Supporting Information). On a point-by-point basis, the simulations of Chla are modestly correlated with the climatology based on remote sensing (Fig.6, correlation coefficient 0.45) and has a much weaker variation (standard deviation less than half that) of the observed field. The two simulations are almost identical in this regard (Fig.6) so Chla comparisons do not discriminate.

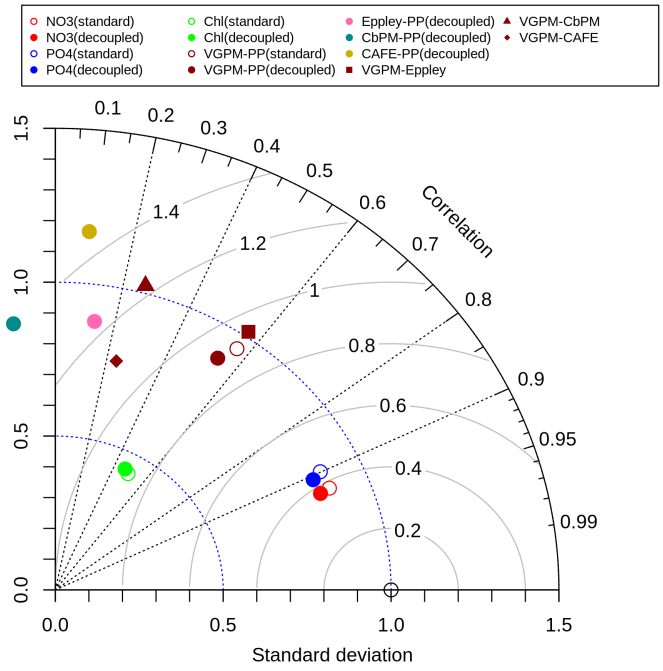

Figure 6. Taylor diagram showing correlations and normalized standard deviations of annual averaged Chla, primary production(PP), nitrate(NO3), and phosphate(PO4) between model simulations (55m depth integrated) and satellited-derived products (Chla and PP) or nutrients from World Ocean Atlas. The circles represent the comparisons between standard simulation and the products, the dots represent the comparisons between decoupled simulation and the products, the square, triangle and diamond represent the comparisons between different satellited-derived primary production. The best match would be a correlation of 1 (on the x axis) and normalized standard deviation of 1 showed as a circle on x axis.

3.3 Global-scale Signatures of Excess Carbon Exudation

The mechanisms and controls on phytoplankton exudation still remain an open question. In these explorations we have assumed that excess photosynthate is produced when photon capture is in excess of growth potential and either accumulates in a "reserve", up to a maximum capacity, or is exuded. The fraction of excess photosynthesis that is exuded $f_{e,j}$, cannot be determined a priori (Eq.11) but in theory can vary between 0 and 1. Different species may also have different $f_{e,j}$. In the results we have shown to this point we set $f_{e,j}$=0.7. Here we examine the sensitivity of, and explain, this choice by running 5 simulations with the decoupled model varying $f_{e,j}$ from 0.1, 0.3, 0.5, 0.7, and 0.9 (Table 2). The global exudation rate increased in proportion to $f_{e,j}$ while the standing stock

of surface DOC increased by 21% in response to a 9-fold increase of $f_{e,j}$. The differences between standard and decoupled simulations here are not only caused by $f_{e,j}$ but also the decoupling of carbon and nutrient flows in primary production (by removing the explicit nutrient limitation, difference of Eq.2 and Eq.3).

Table 2. Surface exudation, DOC, PER, and phytoplankton stoichiometry (55m depth integrated) in different $f_{e,j}$ scenarios.

$f_{e,j}$	**Standard**	**0.1**	**0.3**	**0.5**	**0.7**	**0.9**
Exudation (Pg C/yr)	0.0	1.06	3.31	5.78	8.54	11.78
DOC (Pg C)	1.86	2.48	2.58	2.70	2.83	3.00
Percentage of Extracellular Release	0.0	2.97%	9.13%	15.65%	22.66%	30.40%
C:N	6.62	10.03	9.43	8.79	8.10	7.33
C:P	106.0	160.49	150.88	140.67	129.63	117.27

By decoupling photosynthesis and biosynthesis and allowing extra C storage in cells, the decoupled model (Fig.2b) also resolves a dynamic phytoplankton stoichiometry instead of a fixed one, which leads to a more dynamic and realistic global pattern of particulate C:N and C:P ratios (Fig.7 and S3). The global patterns of particulate (plankton and detrital matter) C:N and C:P ratios could also serve as an indicator of the model performance when comparing with observations. The regions where C:N:P ratios are most affected by $f_{e,j}$ are oligotrophic gyres where photosynthetic rate is usually higher than biosynthesis rate (Fig.S3) and the extra carbon will be either exuded into the environment or retained in the cells. Compared with observations, our decoupled simulations capture the general patterns of global particulate C:N:P ratio (Martiny et al., 2014; Martiny, Pham, et al., 2013; Martiny, Vrugt, et al., 2013): high C:N and C:P ratios in oligotrophic gyres and low C:N and C:P ratios in cold, nutrient rich high latitude regions.

However, the simulation with $f_{e,j} = 0.5$ has higher within region variation than observations especially in subtropical gyres while the simulation of $f_{e,j} = 0.9$ has a much lower variation than observations across the whole global ocean. The results most consistent with the observed C:N:P ratio has $f_{e,j} = 0.7$ (implying that 70% of extra fixed C is exuded and 30% of the extra C is stored in C reserve). And as such, this is the main simulation we have shown in this manuscript.

In the decoupled simulations of $f_{e,j} = 0.7$, the predicted surface exudation rate (0-55m integral) is shown in Fig.8a and the predicted percentage of total C in the C reserve is shown is Fig.8b. As would be expected, the percentage of total phytoplankton carbon in the reserve pool shares a similar spatial pattern with surface exudation, reflecting regions where strong nutrient limitation and high photon fluxes coincide and in accord with previous experimental and modeling studies (Livanou et al., 2019; Flynn et al., 2008; Szul et al., 2019; Braakman, 2019). We quantified the percentage of extracellular release (PER), defined as the percentage of total net photosynthesis released as exudate (shown in Fig.8c). In the model PER is less than 15% in high latitude regions and greater than 50% in subtropical gyres. This pattern is broadly consistent with field studies that reported that PER less than 10% in productive regions with high nutrient concentration and up to 46% in less productive regions like oligotrophic subtropical gyres (Teira, Pazó, et al., 2001; Teira, Serret, & Fernández, 2001; Lagaria et al., 2013). Similarly, in laboratory cultures, PER has been observed to vary between 2% to 10% under nutrient-replete conditions and increase up to 60% in nutrient-deplete conditions (Myklestad, 2000). The global exudation accounted for about 19% of the total global DOC source with the rest originating from death and sloppy feeding. None of these rates are well constrained in the model, reflecting both the simplicity

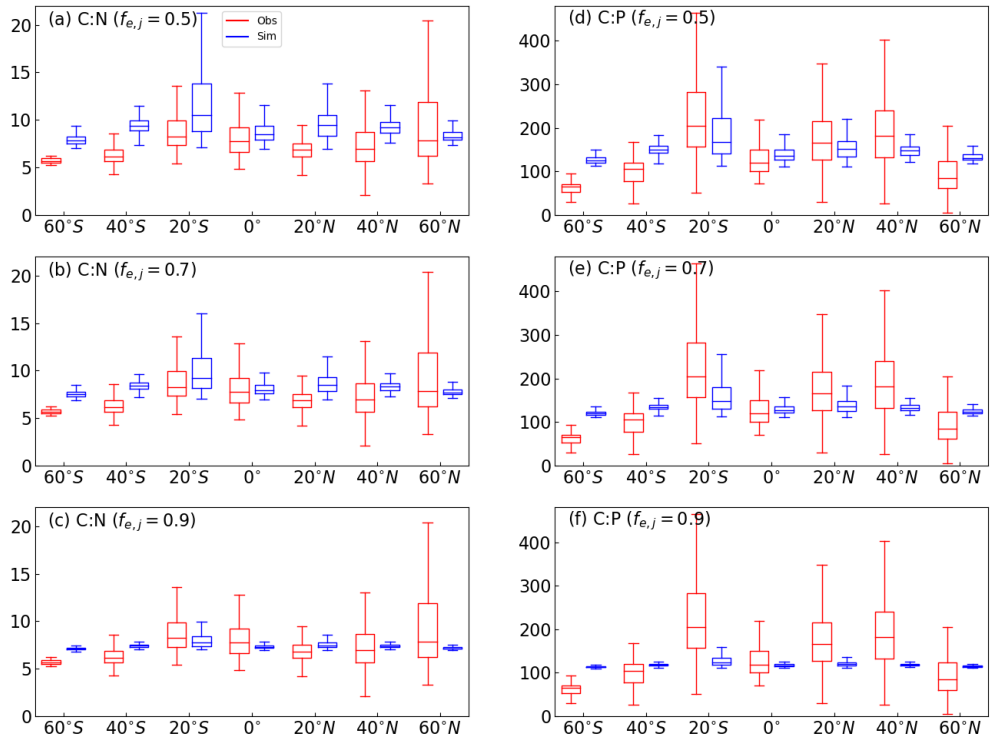

Figure 7. Particulate C:N and C:P ratios in Martiny et al. (2014) (red) and decoupled simulations (blue) with different $f_{e,j}$. The red bars of observations only contain a limited number of observation points while the blue bars of the simulations include all the grid points within each range. (a) to (c) are C:N ratios with $f_{e,j} = 0.5, 0.7, 0.9$, (d) to (f) are C:P ratios with $f_{e,j} = 0.5, 0.7, 0.9$.

of the parameterizations, but also the challenge of a clear and quantitative interpretation of the mechanisms at laboratory work.

4 Summary and Outlook

We have examined the consequences of the tight coupling of nutrient availability and photosynthesis in a commonly employed parameterization (Geider et al., 1997) for regional and global-scale carbon cycle simulations. The decoupling of these two processes significantly improved simulations of the vertical profile of subtropical primary productivity when compared to in situ observations. In global simulations, it increased integrated primary production by about one-third with the most impact in oligotrophic subtropical gyres where the original formulation with coupled processes consistently underestimated primary production relative to many satellite-based estimates. However, we note the large uncertainty in the large scale satellite based estimates (see e.g. Fig 6, Carr et al. (2006)).

In order to explore the sensitivity of regional and global-scale simulations we have assumed either complete coupling or decoupling of photosynthesis/biosynthesis. It is likely that neither extreme is fully realistic and Geider et al. (1997) were clear about the uncertainty associated with the coupled assumption. There are numerous ways in which phytoplankton can accommodate light intensities greater than required to satisfy biosynthesis constraints, including the production of photo-protective pigments and photo-respiration (Halsey & Jones, 2015) which have not been considered here. This study provides a clear

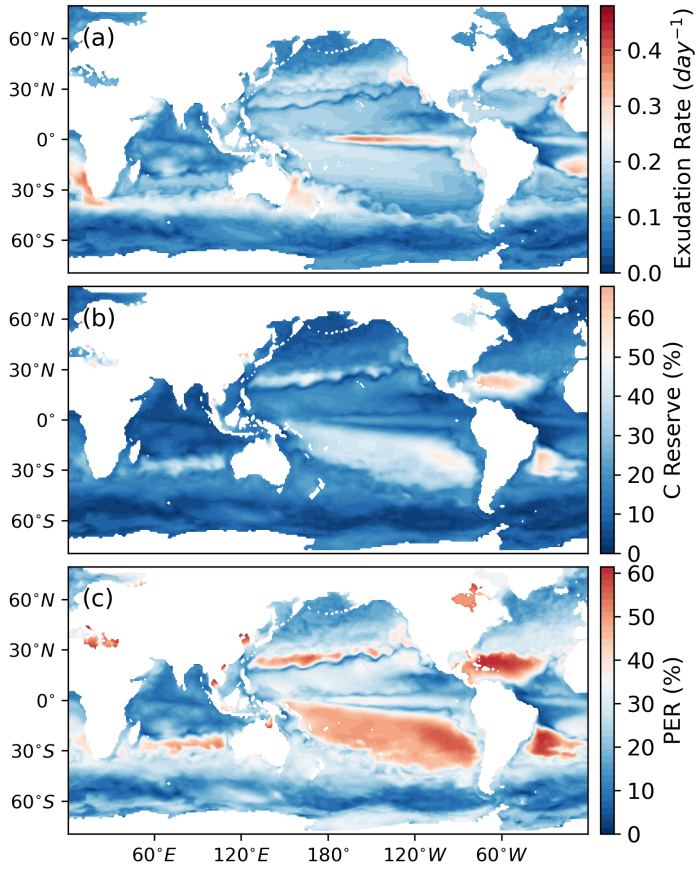

Figure 8. Global exudation rate, C reserve, and percentage of extracellular release patterns (55m depth integrated). (a) simulated exudation rate (day^{-1}), (b) Percentage of total C in C reserve (%), (c) Percentage extracellular release (%).

indication of the sensitivity to two extreme possibilities and shows that they do have major implications for the simulation of global-scale productivity and the production of DOC. Most compellingly, the simulations demonstrate that the vertical profile of primary production in oligotrophic environments is significantly improved in the decoupled case, bringing the simulations into agreement with observed profiles of primary production and Chla at HOT and BATS. As a consequence we suggest that the decoupled approach is the better candidate for global carbon cycle simulations at present. In the global 3D simulation this new parameterization increased globally-integrated, annual primary production by about a third. Such changes could have significant impact on how models capture the cycling of carbon in the upper ocean, and such processes may have an impact on their ability to capture inter-annual and longer term changes in the carbon cycle.

As a point of discussion, we found that the improvement in the vertical profile of simulations was more significant in the 1D simulation when vertically resolution is higher. In other words, if the euphotic layer is represented coarsely (i.e. greater than 10m resolution), the low surface productivity associated with the standard approach is not easily apparent because the profile is not resolved. As climate and carbon cycle models increase in both horizontal and vertical resolution with increasing computational resources, the issue will be more apparent. That said, even at coarse vertical resolution in the 3D simulations, the lower global primary production of the standard approach could represent a problem. Moreover,

if models using the standard approach have been tuned to have reasonable global primary productions, they may in fact overestimate biosynthetic rates (if simulated).

Allocation of excess photosynthate to the reserve increases simulated C:N and C:P ratios of particulate matter, particularly in the subtropics. Depending on the choice of parameter values for the amount of carbon exuded versus stored, these increases in the subtropics brought the model more into line with observations (Martiny et al., 2014), and thus may provide an empirical, large-scale calibration. Allocation of all excess photosynthate to exudation would imply an additional source of DOC of more than 12 $Pg\ C\ yr^{-1}$. Allocation of all excess photosynthate to reserves would imply a global increase in C:N from 6.6:1 (Redfield Ratio) to greater than 10:1. A systematic and quantitative data-model synthesis might be employed to better constrain this allocation at the community level, though the complexities and uncertainties of DOC dynamics still clouds the development of suitable parameterizations. Additionally, here we used a uniform parameter $f_{e,j}$ for both types of phytoplankton to control the allocation of excess photosynthate which could be species specific in future simulations. It is likely that different species would have different values, and that these may be altered under different environmental conditions.

In summary, we examined the consequence of decoupling photosynthesis and biosynthesis in the parameterization of photosynthesis employed in global biogeochemical models. We found that removing direct nutrient limitation to photosynthesis significantly improved the simulations of vertical profiles of primary production in the subtropical gyres and increased predicted global primary production by more than 30% relative to the case where photosynthesis and biosynthesis were tightly coupled. We explored the consequences of retention versus exudation of the excess photosynthate in the global simulations which allowed this new model to have reasonable global patterns of C:N and C:P ratios in phytoplankton.

Acknowledgments

We are grateful for the support by the Simons Collaboration on Ocean Processes and Ecology (SCOPE, 329108 to MJF and AW) and Simons Collaboration on Computational Biogeochemical Modeling of Marine Ecosystems (CBIOMES, 549931 to MJF). Additional support is provided by the NSF to the HOT program (OCE-1756517 to AW), the Human Frontiers Science Program (RGP0020/2016 to DS). We also thank the dedicated efforts of the HOT and BATS teams who facilitated in situ sample collection. The code and configurations of the models used in this paper can be found at `https://doi.org/10.6084/m9.figshare.13564229`.

References

Aumont, O., Ethé, C., Tagliabue, A., Bopp, L., & Gehlen, M. (2015). PISCES-v2: An ocean biogeochemical model for carbon and ecosystem studies. *Geoscientific Model Development*, *8*(8), 2465–2513. Retrieved from `www.geosci-model-dev.net/8/2465/2015/` doi: 10.5194/gmd-8-2465-2015

Behrenfeld, M. J., & Falkowski, P. G. (1997, 1). Photosynthetic rates derived from satellite-based chlorophyll concentration. *Limnology and Oceanography*, *42*(1), 1–20. Retrieved from `http://doi.wiley.com/10.4319/lo.1997.42.1.0001` doi: 10.4319/lo.1997.42.1.0001

Berman, T., & Holm-Hansen, O. (1974). Release of photoassimilated carbon as dissolved organic matter by marine phytoplankton. *Marine Biology*, *28*(4), 305–310. Retrieved from `http://link.springer.com/10.1007/BF00388498` doi: 10.1007/BF00388498

Bertlisson, S., Berglund, O., Pullin, M. J., & Chisholm, S. W. (2005). Release of dissolved organic matter by Prochlorococcus. *Vie et Milieu*, *55*(3-4), 225–232.

Bjørrisen, P. K. (1988, 1). *Phytoplankton exudation of organic matter: Why do healthy cells do it?* (Vol. 33) (No. 1). John Wiley & Sons, Ltd. Retrieved from `http://doi.wiley.com/10.4319/lo.1988.33.1.0151` doi: 10.4319/lo.1988.33.1.0151

Braakman, R. (2019, 5). *Evolution of cellular metabolism and the rise of a globally productive biosphere.* Retrieved from `https://linkinghub.elsevier.com/retrieve/pii/S0891584918316897` doi: 10.1016/j.freeradbiomed.2019.05.004

Braakman, R., Follows, M. J., & Chisholm, S. W. (2017). Metabolic evolution and the self-organization of ecosystems. *Proceedings of the National Academy of Sciences*, *114*(15), E3091-E3100. Retrieved from `http://www.pnas.org/lookup/doi/10.1073/pnas.1619573114` doi: 10.1073/pnas.1619573114

Bruggeman, J., & Kooijman, S. A. (2007, 7). A biodiversity-inspired approach to aquatic ecosystem modeling. *Limnology and Oceanography*, *52*(4), 1533–1544. Retrieved from `http://doi.wiley.com/10.4319/lo.2007.52.4.1533` doi: 10.4319/lo.2007.52.4.1533

Cailliau, C., Claustre, H., Vidussi, F., Marie, D., & Vaulot, D. (1996, 12). Carbon biomass, and gross growth rates as estimated from 14C pigment labelling, during photoacclimation in Prochlorococcus CCMP 1378. *Marine Ecology Progress Series*, *145*(1-3), 209–221. Retrieved from `http://www.int-res.com/abstracts/meps/v145/p209-221/` doi: 10.3354/meps145209

Carr, M. E., Friedrichs, M. A., Schmeltz, M., Noguchi Aita, M., Antoine, D., Arrigo, K. R., ... Yamanaka, Y. (2006). A comparison of global estimates of marine primary production from ocean color. *Deep-Sea Research Part II: Topical Studies in Oceanography*, *53*(5-7), 741–770. doi: 10.1016/j.dsr2.2006.01.028

Cavender-Bares, K. K., Karl, D. M., & Chisholm, S. W. (2001). Nutrient gradients in the western North Atlantic Ocean: Relationship to microbial community structure and comparison to patterns in the Pacific Ocean. *Deep-Sea Research Part I: Oceanographic Research Papers*, *48*(11), 2373–2395. doi: 10.1016/S0967-0637(01)00027-9

Dunne, J. P., John, J. G., Shevliakova, S., Stouffer, R. J., Krasting, J. P., Malyshev, S. L., ... Zadeh, N. (2013, 4). GFDL's ESM2 global coupled climate-carbon earth system models. Part II: Carbon system formulation and baseline simulation characteristics.

Journal of Climate, *26*(7), 2247–2267. Retrieved from http://journals.ametsoc.org/doi/abs/10.1175/JCLI-D-12-00150.1 doi: 10.1175/JCLI-D-12-00150.1

Dutkiewicz, S., Cermeno, P., Jahn, O., Follows, M. J., Hickman, A. A., Taniguchi, D. A., & Ward, B. A. (2020, 2). Dimensions of marine phytoplankton diversity. *Biogeosciences*, *17*(3), 609–634. Retrieved from https://www.biogeosciences.net/17/609/2020/ doi: 10.5194/bg-17-609-2020

Dutkiewicz, S., Hickman, A. E., Jahn, O., Gregg, W. W., Mouw, C. B., & Follows, M. J. (2015, 7). Capturing optically important constituents and properties in a marine biogeochemical and ecosystem model. *Biogeosciences*, *12*(14), 4447–4481. Retrieved from https://www.biogeosciences.net/12/4447/2015/ doi: 10.5194/bg-12-4447-2015

Field, C. B., Behrenfeld, M. J., Randerson, J. T., & Falkowski, P. (1998, 7). Primary production of the biosphere: Integrating terrestrial and oceanic components. *Science*, *281*(5374), 237–240. doi: 10.1126/science.281.5374.237

Flynn, K. J. (2003, 2). *Modelling multi-nutrient interactions in phytoplankton; balancing simplicity and realism* (Vol. 56) (No. 2). Elsevier Ltd. doi: 10.1016/S0079-6611(03)00006-5

Flynn, K. J., Clark, D. R., & Xue, Y. (2008, 10). Modeling the release of dissolved organic matter by phytoplankton. *Journal of Phycology*, *44*(5), 1171–1187. Retrieved from http://doi.wiley.com/10.1111/j.1529-8817.2008.00562.x doi: 10.1111/j.1529-8817.2008.00562.x

Follows, M. J., Dutkiewicz, S., Grant, S., & Chisholm, S. W. (2007, 3). Emergent biogeography of microbial communities in a model ocean. *Science*, *315*(5820), 1843–1846. Retrieved from http://www.ncbi.nlm.nih.gov/pubmed/17395828 doi: 10.1126/science.1138544

Garcia, H. E., Locarnini, R. A., Boyer, T. P., Antonov, J. I., Baranova, O. K., Zweng, M. M., ... Johnson, D. R. (2018). *World Ocean Atlas 2018, Volume 4 : Dissolved Inorganic Nutrients (phosphate, nitrate and and nitrate+nitrite, silicate)* (Vol. 4) (No. July). Retrieved from https://www.nodc.noaa.gov/OC5/woa18/pubwoa18.html

Geider, R. J., MacIntyre, H. L., & Kana, T. M. (1997). Dynamic model of phytoplankton growth and acclimation: Responses of the balanced growth rate and the chlorophyll a:carbon ratio to light, nutrient-limitation and temperature. *Marine Ecology Progress Series*, *148*(1-3), 187–200. Retrieved from https://www.int-res.com/articles/meps/148/m148p187.pdf doi: 10.3354/meps148187

Grossowicz, M., Marques, G. M., & van Voorn, G. A. (2017, 9). A dynamic energy budget (DEB) model to describe population dynamics of the marine cyanobacterium Prochlorococcus marinus. *Ecological Modelling*, *359*, 320–332. doi: 10.1016/j.ecolmodel.2017.06.011

Grossowicz, M., Roth-Rosenberg, D., Aharonovich, D., Silverman, J., Follows, M. J., & Sher, D. (2017, 3). Prochlorococcus in the lab and in silico: The importance of representing exudation. *Limnology and Oceanography*, *62*(2), 818–835. Retrieved from http://doi.wiley.com/10.1002/lno.10463 doi: 10.1002/lno.10463

Halsey, K. H., & Jones, B. M. (2015, 1). Phytoplankton Strategies for Photosynthetic Energy Allocation. *Annual Review of Marine Science*, *7*(1), 265–297. Retrieved from http://www.annualreviews.org/doi/10.1146/annurev-marine-010814-015813 doi: 10.1146/annurev-marine-010814-015813

Hickman, A. E., Dutkiewicz, S., Williams, R. G., & Follows, M. J. (2010, 5). Modelling the effects of chromatic adaptation on phytoplankton community structure in the oligotrophic ocean. *Marine Ecology Progress Series*, *406*, 1–17. doi: 10.3354/meps08588

Karl, D. M., & Church, M. J. (2014). *Microbial oceanography and the Hawaii Ocean Time-series programme* (Vol. 12) (No. 10). Retrieved from www.nature.com/reviews/micro doi: 10.1038/nrmicro3333

Kulk, G., de Poll, W. H., Visser, R. J., & Buma, A. G. (2011, 2). Distinct differences in photoacclimation potential between prokaryotic and eukaryotic oceanic phytoplankton. *Journal of Experimental Marine Biology and Ecology*, *398*(1-2),

63–72. Retrieved from https://www.sciencedirect.com/science/article/pii/S0022098110005101 doi: 10.1016/j.jembe.2010.12.011

Lagaria, A., Psarra, S., Gogou, A., Turul, S., & Christaki, U. (2013, 6). Particulate and dissolved primary production along a pronounced hydrographic and trophic gradient (Turkish Straits System-NE Aegean Sea). *Journal of Marine Systems*, *119-120*, 1–10. doi: 10.1016/j.jmarsys.2013.02.009

Letelier, R. M., Dore, J. E., Winn, C. D., & Karl, D. M. (1996, 1). Seasonal and interannual variations in photosynthetic carbon assimilation at station ALOHA. *Deep-Sea Research Part II: Topical Studies in Oceanography*, *43*(2-3), 467–490. doi: 10.1016/0967-0645(96)00006-9

Letelier, R. M., Karl, D. M., Abbott, M. R., & Bidigare, R. R. (2004, 3). Light driven seasonal patterns of chlorophyll and nitrate in the lower euphotic zone of the North Pacific Subtropical Gyre. *Limnology and Oceanography*, *49*(2), 508–519. Retrieved from https://aslopubs.onlinelibrary.wiley.com/doi/full/10.4319/lo.2004.49.2.0508https://aslopubs.onlinelibrary.wiley.com/doi/abs/10.4319/lo.2004.49.2.0508https://aslopubs.onlinelibrary.wiley.com/doi/10.4319/lo.2004.49.2.0508 doi: 10.4319/lo.2004.49.2.0508

Letelier, R. M., White, A. E., Bidigare, R. R., Barone, B., Church, M. J., & Karl, D. M. (2017). Light absorption by phytoplankton in the North Pacific Subtropical Gyre. *Limnology and Oceanography*, *62*(4), 1526–1540. doi: 10.1002/lno.10515

Livanou, E., Lagaria, A., Psarra, S., & Lika, K. (2019, 1). A DEB-based approach of modeling dissolved organic matter release by phytoplankton. *Journal of Sea Research*, *143*, 140–151. Retrieved from https://www.sciencedirect.com/science/article/pii/S1385110118300303 doi: 10.1016/j.seares.2018.07.016

López-Sandoval, D. C., Rodríguez-Ramos, T., Cermeño, P., & Marañón, E. (2013, 3). Exudation of organic carbon by marine phytoplankton: Dependence on taxon and cell size. *Marine Ecology Progress Series*, *477*, 53–60. doi: 10.3354/meps10174

Luo, C., Mahowald, N., Bond, T., Chuang, P. Y., Artaxo, P., Siefert, R., ... Schauer, J. (2008, 3). Combustion iron distribution and deposition. *Global Biogeochemical Cycles*, *22*(1). doi: 10.1029/2007GB002964

Mackey, K. R., Paytan, A., Grossman, A. R., & Bailey, S. (2008, 5). A photosynthetic strategy for coping in a high-light, low-nutrient environment. *Limnology and Oceanography*, *53*(3), 900–913. Retrieved from http://doi.wiley.com/10.4319/lo.2008.53.3.0900 doi: 10.4319/lo.2008.53.3.0900

Malmstrom, R. R., Coe, A., Kettler, G. C., Martiny, A. C., Frias-Lopez, J., Zinser, E. R., & Chisholm, S. W. (2010). Temporal dynamics of Prochlorococcus ecotypes in the Atlantic and pacific oceans. *ISME Journal*, *4*(10), 1252–1264. Retrieved from http://dx.doi.org/10.1038/ismej.2010.60 doi: 10.1038/ismej.2010.60

Marañón, E., Cermeño, P., López-Sandoval, D. C., Rodríguez-Ramos, T., Sobrino, C., Huete-Ortega, M., ... Rodríguez, J. (2013). Unimodal size scaling of phytoplankton growth and the size dependence of nutrient uptake and use. *Ecology Letters*, *16*(3), 371–379. Retrieved from https://onlinelibrary.wiley.com/doi/pdf/10.1111/ele.12052 doi: 10.1111/ele.12052

Marshall, J., Adcroft, A., Hill, C., Perelman, L., & Heisey, C. (1997). A finite-volume, incompressible navier stokes model for, studies of the ocean on parallel computers. *Journal of Geophysical Research C: Oceans*, *102*(C3), 5753–5766. doi: 10.1029/96JC02775

Martin, P., Dyhrman, S. T., Lomas, M. W., Poulton, N. J., & Van Mooy, B. A. (2014, 6). Accumulation and enhanced cycling of polyphosphate by Sargasso Sea plankton in response to low phosphorus. *Proceedings of the National Academy of Sciences of the United States of America*, *111*(22), 8089–8094. doi: 10.1073/pnas.1321719111

Martiny, A. C., Pham, C. T., Primeau, F. W., Vrugt, J. A., Moore, J. K., Levin, S. A., & Lomas, M. W. (2013, 4). Strong latitudinal patterns in the elemental ratios of marine plankton and organic matter. *Nature Geoscience*, *6*(4), 279–283. Retrieved from www.nature.com/naturegeoscience doi: 10.1038/ngeo1757

Martiny, A. C., Vrugt, J. A., & Lomas, M. W. (2014, 12). Concentrations and ratios of

particulate organic carbon, nitrogen, and phosphorus in the global ocean. *Scientific Data*, *1*(1), 1–7. Retrieved from www.nature.com/scientificdata doi: 10.1038/sdata.2014.48

Martiny, A. C., Vrugt, J. A., Primeau, F. W., & Lomas, M. W. (2013, 9). Regional variation in the particulate organic carbon to nitrogen ratio in the surface ocean. *Global Biogeochemical Cycles*, *27*(3), 723–731. Retrieved from https://agupubs.onlinelibrary.wiley.com/doi/full/10.1002/gbc.20061https://agupubs.onlinelibrary.wiley.com/doi/abs/10.1002/gbc.20061https://agupubs.onlinelibrary.wiley.com/doi/10.1002/gbc.20061 doi: 10.1002/gbc.20061

McGillicuddy, D. J. (2016, 1). Mechanisms of Physical-Biological-Biogeochemical Interaction at the Oceanic Mesoscale. *Annual Review of Marine Science*, *8*(1), 125–159. Retrieved from http://www.annualreviews.org/doi/10.1146/annurev-marine-010814-015606 doi: 10.1146/annurev-marine-010814-015606

Myklestad, S. M. (2000, 9). Dissolved Organic Carbon from Phytoplankton. In *Marine chemistry* (pp. 111–148). Springer-Verlag. doi: 10.1007/10683826{_}5

Roth-Rosenberg, D., Aharonovich, D., Omta, A. W., Follows, M. J., & Sher, D. (2021). Dynamic macromolecular composition and high exudation rates in Prochlorococcus. *bioRxiv*, 828897. Retrieved from https://doi.org/10.1101/828897 doi: 10.1101/828897

Sarmento, H., Morana, C., & Gasol, J. M. (2016, 11). Bacterioplankton niche partitioning in the use of phytoplankton-derived dissolved organic carbon: Quantity is more important than quality. *ISME Journal*, *10*(11), 2582–2592. Retrieved from http://www.nature.com/articles/ismej201666 doi: 10.1038/ismej.2016.66

Silsbe, G. M., Behrenfeld, M. J., Halsey, K. H., Milligan, A. J., & Westberry, T. K. (2016). The CAFE model: A net production model for global ocean phytoplankton. *Global Biogeochemical Cycles*, *30*(12), 1756–1777. Retrieved from http://www.science.oregonstate.edu/ocean.productivity/. doi: 10.1002/2016GB005521

Steinberg, D. K., Carlson, C. A., Bates, N. R., Johnson, R. J., Michaels, A. F., & Knap, A. H. (2001, 1). Overview of the US JGOFS Bermuda Atlantic Time-series Study (BATS): A decade-scale look at ocean biology and biogeochemistry. *Deep-Sea Research Part II: Topical Studies in Oceanography*, *48*(8-9), 1405–1447. doi: 10.1016/S0967-0645(00)00148-X

Szeto, M., Werdell, P. J., Moore, T. S., & Campbell, J. W. (2011, 10). Are the world's oceans optically different? *Journal of Geophysical Research: Oceans*, *116*(10), C00H04. Retrieved from http://doi.wiley.com/10.1029/2011JC007230 doi: 10.1029/2011JC007230

Szul, M. J., Dearth, S. P., Campagna, S. R., & Zinser, E. R. (2019). Carbon Fate and Flux in Prochlorococcus under Nitrogen Limitation. *mSystems*, *4*(1). Retrieved from http://msystems.asm.org/ doi: 10.1128/msystems.00254-18

Talmy, D., Blackford, J., Hardman-Mountford, N. J., Polimene, L., Follows, M. J., & Geider, R. J. (2014, 9). Flexible C : N ratio enhances metabolism of large phytoplankton when resource supply is intermittent. *Biogeosciences*, *11*(17), 4881–4895. Retrieved from https://www.biogeosciences.net/11/4881/2014/ doi: 10.5194/bg-11-4881-2014

Taylor, K. E. (2001, 4). Summarizing multiple aspects of model performance in a single diagram. *Journal of Geophysical Research Atmospheres*, *106*(D7), 7183–7192. Retrieved from https://agupubs.onlinelibrary.wiley.com/doi/full/10.1029/2000JD900719https://agupubs.onlinelibrary.wiley.com/doi/abs/10.1029/2000JD900719https://agupubs.onlinelibrary.wiley.com/doi/10.1029/2000JD900719 doi: 10.1029/2000JD900719

Teira, E., Pazó, M. J., Serret, P., & Fernández, E. (2001, 9). Dissolved organic carbon production by microbial populations in the Atlantic Ocean. *Limnology and Oceanography*, *46*(6), 1370–1377. Retrieved from http://doi.wiley.com/10.4319/lo.2001.46.6.1370 doi: 10.4319/lo.2001.46.6.1370

Teira, E., Serret, P., & Fernández, E. (2001). Phytoplankton size-structure, particulate and

dissolved organic carbon production and oxygen fluxes through microbial communities in the NW Iberian coastal transition zone. *Marine Ecology Progress Series*, *219*, 65–83. Retrieved from http://www.int-res.com/abstracts/meps/v219/p65-83/ doi: 10.3354/meps219065

Thompson, A. W., van den Engh, G., Ahlgren, N. A., Kouba, K., Ward, S., Wilson, S. T., & Karl, D. M. (2018, 12). Dynamics of Prochlorococcus Diversity and Photoacclimation During Short-Term Shifts in Water Column Stratification at Station ALOHA. *Frontiers in Marine Science*, *5*, 488. Retrieved from https://www.frontiersin.org/article/10.3389/fmars.2018.00488/full doi: 10.3389/fmars.2018.00488

Thornton, D. C. (2014). Dissolved organic matter (DOM) release by phytoplankton in the contemporary and future ocean. *European Journal of Phycology*, *49*(1), 20–46. Retrieved from http://dx.doi.org/10.1080/09670262.2013.875596 doi: 10.1080/09670262.2013.875596

Vallino, J. J. (2000, 1). Improving marine ecosystem models: Use of data assimilation and mesocosm experiments. *Journal of Marine Research*, *58*(1), 117–164. Retrieved from http://www.ingentaselect.com/rpsv/cgi-bin/cgi?ini=xref&body=linker&reqdoi=10.1357/002224000321511223 doi: 10.1357/002224000321511223

Ward, B. A., Dutkiewicz, S., Jahn, O., & Follows, M. J. (2012). A size-structured food-web model for the global ocean. *Limnology and Oceanography*, *57*(6), 1877–1891. doi: 10.4319/lo.2012.57.6.1877

Ward, B. A., & Follows, M. J. (2016, 3). Marine mixotrophy increases trophic transfer efficiency, mean organism size, and vertical carbon flux. *Proceedings of the National Academy of Sciences*, *113*(11), 2958–2963. Retrieved from http://www.pnas.org/lookup/doi/10.1073/pnas.1517118113http://www.ncbi.nlm.nih.gov/pubmed/26831076http://www.pubmedcentral.nih.gov/articlerender.fcgi?artid=PMC4801304 doi: 10.1073/pnas.1517118113

Westberry, T., Behrenfeld, M. J., Siegel, D. A., & Boss, E. (2008, 6). Carbon-based primary productivity modeling with vertically resolved photoacclimation. *Global Biogeochemical Cycles*, *22*(2), n/a-n/a. Retrieved from http://doi.wiley.com/10.1029/2007GB003078 doi: 10.1029/2007GB003078

White, A. E., Letelier, R. M., Whitmire, A. L., Barone, B., Bidigare, R. R., Church, M. J., & Karl, D. M. (2015, 11). Phenology of particle size distributions and primary productivity in the North Pacific subtropical gyre (Station ALOHA). *Journal of Geophysical Research: Oceans*, *120*(11), 7381–7399. Retrieved from https://onlinelibrary.wiley.com/doi/abs/10.1002/2015JC010897 doi: 10.1002/2015JC010897

Wunsch, C., & Heimbach, P. (2007). Practical global oceanic state estimation. *Physica D: Nonlinear Phenomena*, *230*(1-2), 197–208. doi: 10.1016/j.physd.2006.09.040

Figure 1.

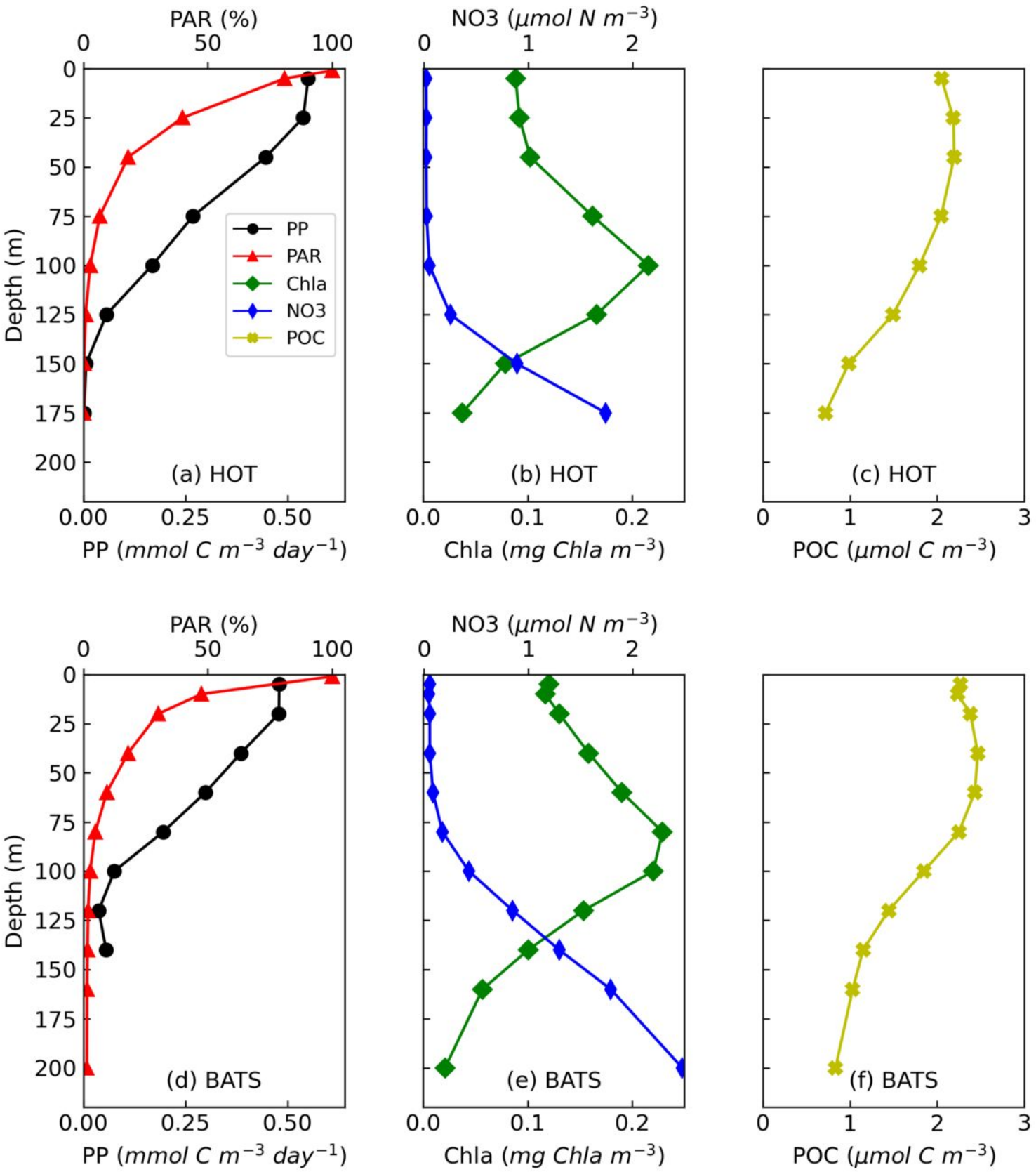
PAR (%)
NO3 ($\mu mol\ N\ m^{-3}$)
Depth (m)
PP
PAR
Chla
NO3
POC
(a) HOT
(b) HOT
(c) HOT
(d) BATS
(e) BATS
(f) BATS
PP ($mmol\ C\ m^{-3}\ day^{-1}$)
Chla ($mg\ Chla\ m^{-3}$)
POC ($\mu mol\ C\ m^{-3}$)

Figure 2.

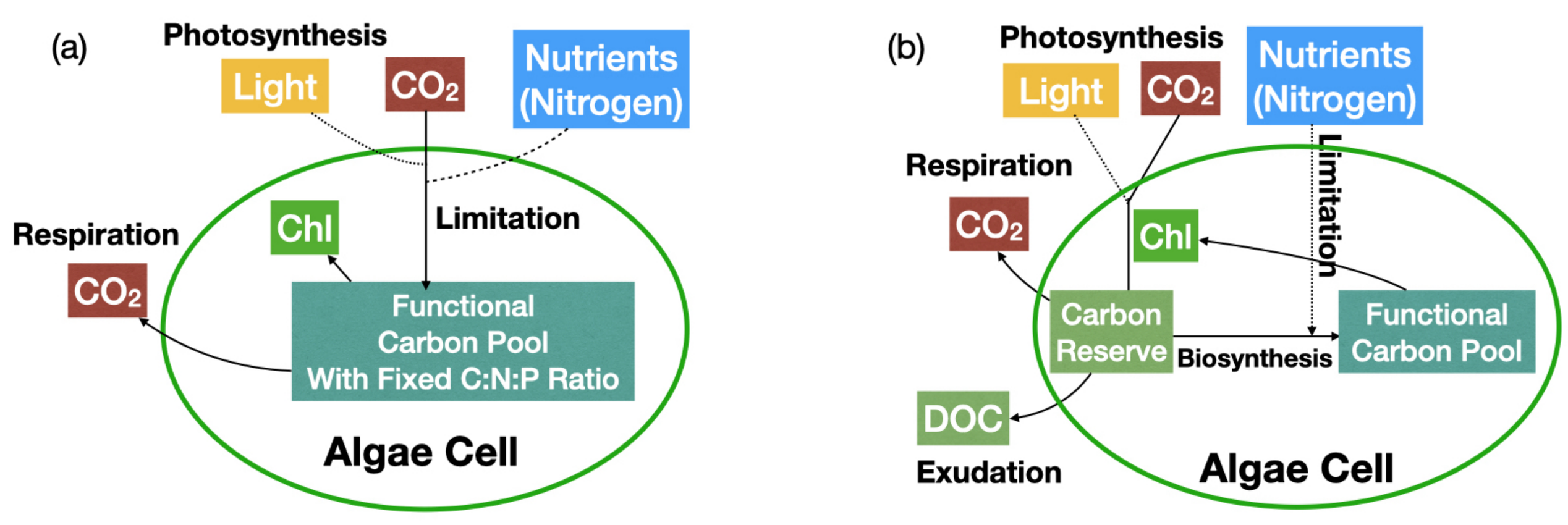
(a)
Photosynthesis
Light
CO_2
Nutrients (Nitrogen)
Chl
Limitation
Respiration
CO_2
Functional Carbon Pool With Fixed C:N:P Ratio
Algae Cell
(b)
Photosynthesis
Light
CO_2
Nutrients (Nitrogen)
Respiration
CO_2
Chl
Limitation
Carbon Reserve
Biosynthesis
Functional Carbon Pool
DOC
Exudation
Algae Cell

Figure 3.

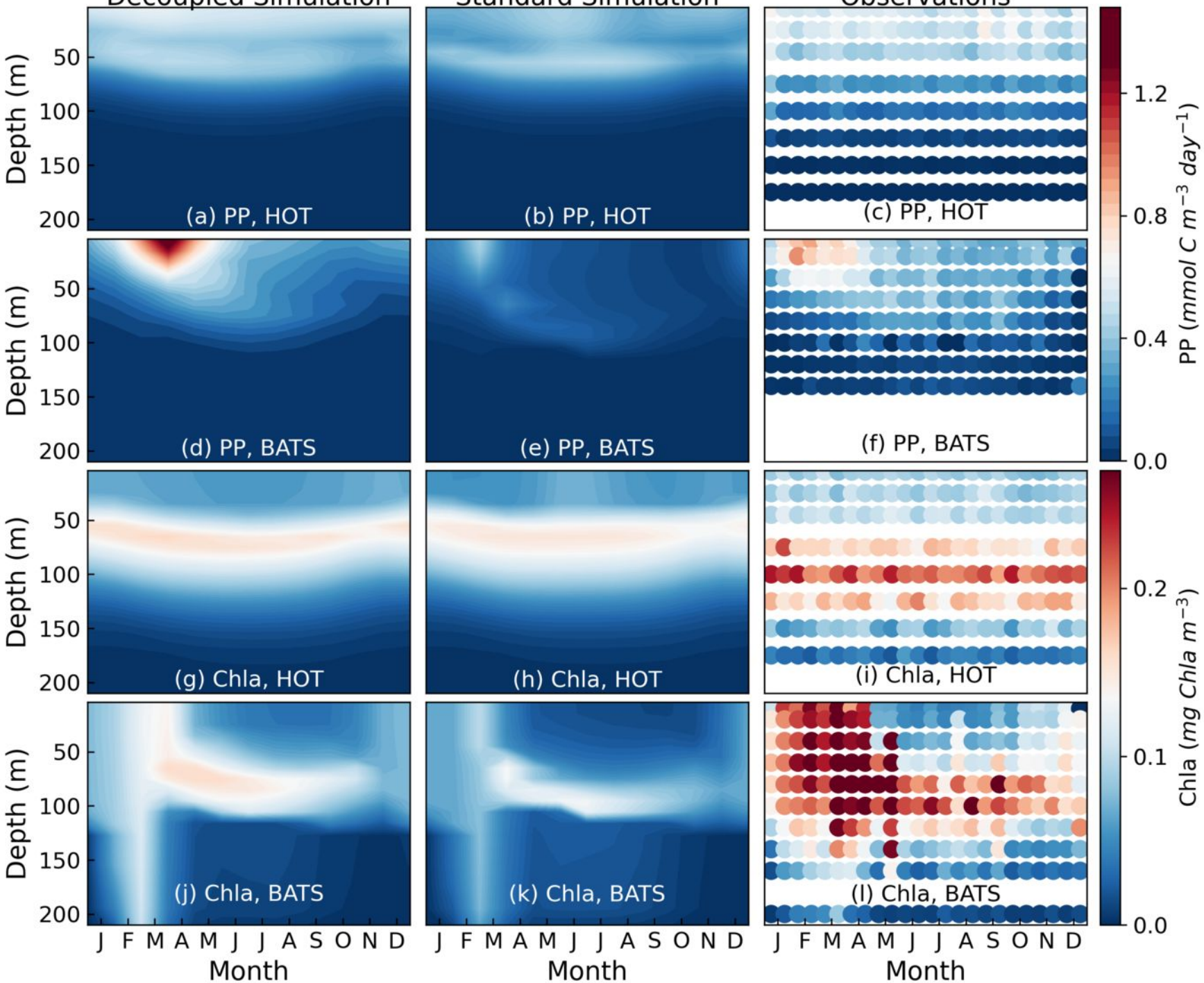
Decoupled Simulation
Standard Simulation
Observations
Depth (m)
50
100
150
200
(a) PP, HOT
(b) PP, HOT
(c) PP, HOT
(d) PP, BATS
(e) PP, BATS
(f) PP, BATS
(g) Chla, HOT
(h) Chla, HOT
(i) Chla, HOT
(j) Chla, BATS
(k) Chla, BATS
(l) Chla, BATS
J F M A M J J A S O N D
Month
PP (mmol C m−3 day−1)
0.0
0.4
0.8
1.2
Chla (mg Chla m−3)
0.0
0.1
0.2

Figure 4.

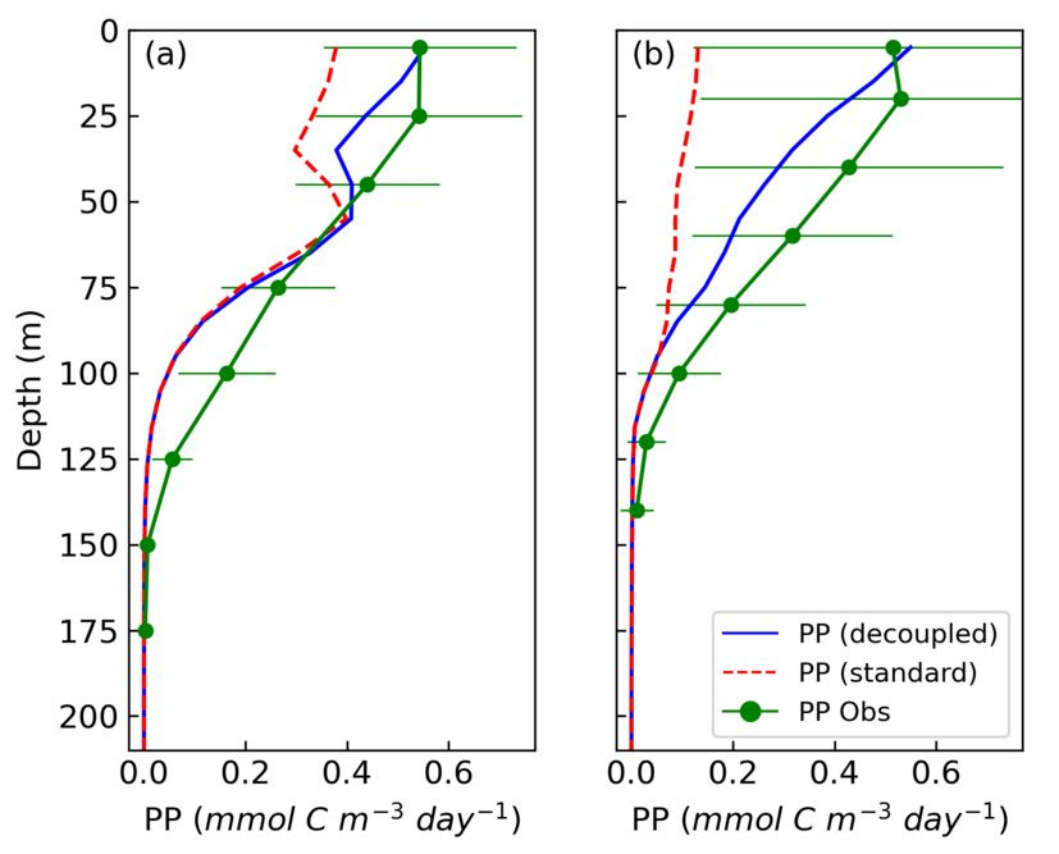
(a)
(b)
Depth (m)
0
25
50
75
100
125
150
175
200
0.0
0.2
0.4
0.6
PP (mmol C m^{-3} day^{-1})
PP (decoupled)
PP (standard)
PP Obs

Figure 5.

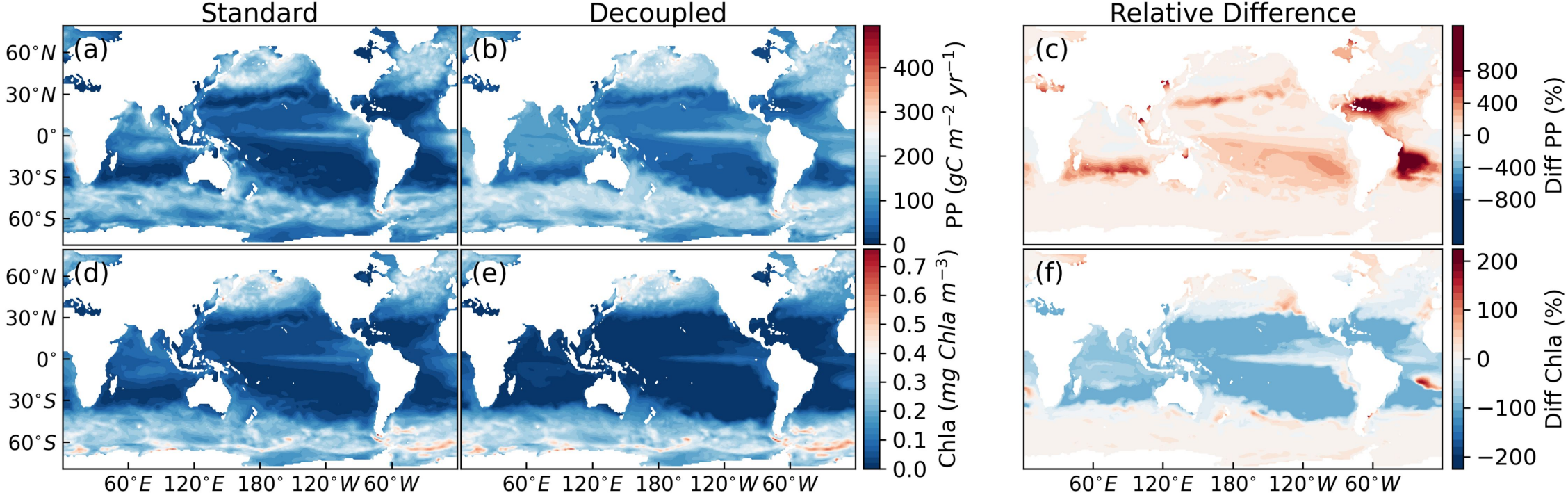
Standard
Decoupled
Relative Difference
(a)
(b)
(c)
(d)
(e)
(f)
60°N
30°N
0°
30°S
60°S
60°E
120°E
180°
120°W
60°W
PP (gC m−2 yr−1)
0
100
200
300
400
Chla (mg Chla m−3)
0.0
0.1
0.2
0.3
0.4
0.5
0.6
0.7
Diff PP (%)
−800
−400
0
400
800
Diff Chla (%)
−200
−100
0
100
200

Figure 6.

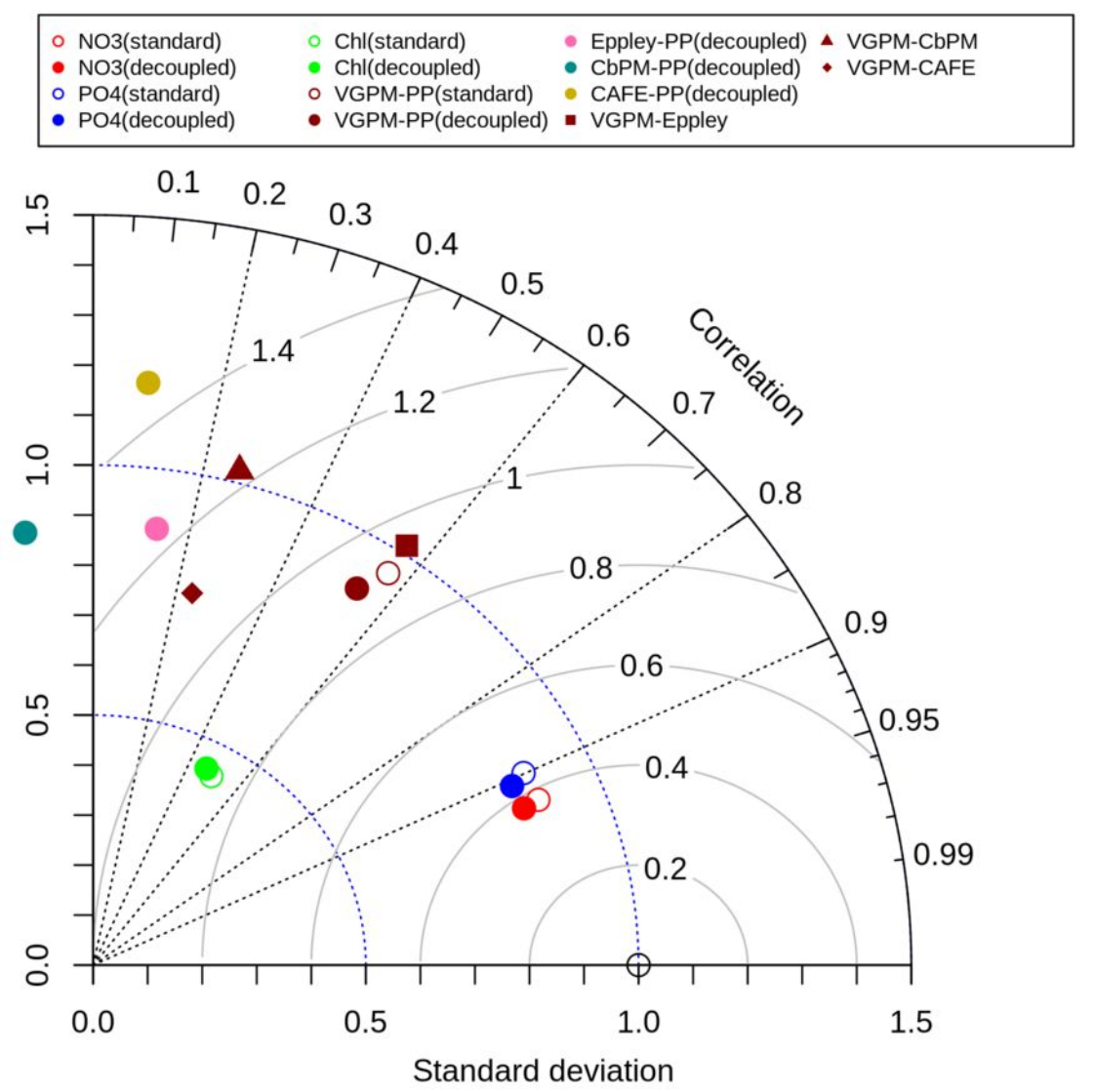
NO3(standard)
NO3(decoupled)
PO4(standard)
PO4(decoupled)
Chl(standard)
Chl(decoupled)
VGPM-PP(standard)
VGPM-PP(decoupled)
Eppley-PP(decoupled)
CbPM-PP(decoupled)
CAFE-PP(decoupled)
VGPM-Eppley
VGPM-CbPM
VGPM-CAFE
Correlation
0.1
0.2
0.3
0.4
0.5
0.6
0.7
0.8
0.9
0.95
0.99
1.4
1.2
1
0.8
0.6
0.4
0.2
0.0
0.5
1.0
1.5
Standard deviation

Figure 7.

(a) C:N ($f_{e,j} = 0.5$)

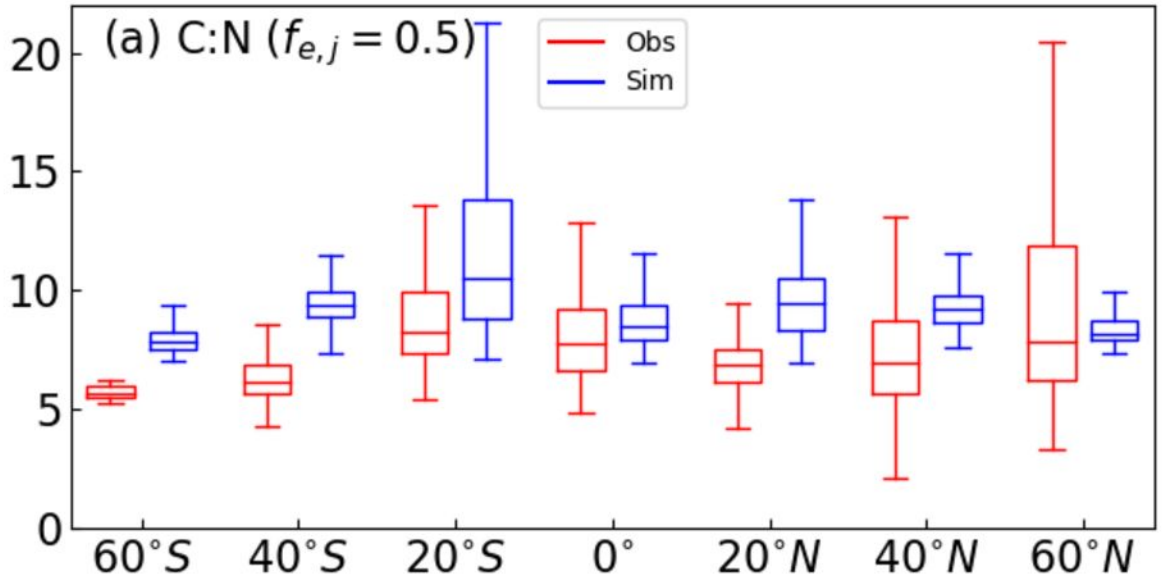

(d) C:P ($f_{e,j} = 0.5$)

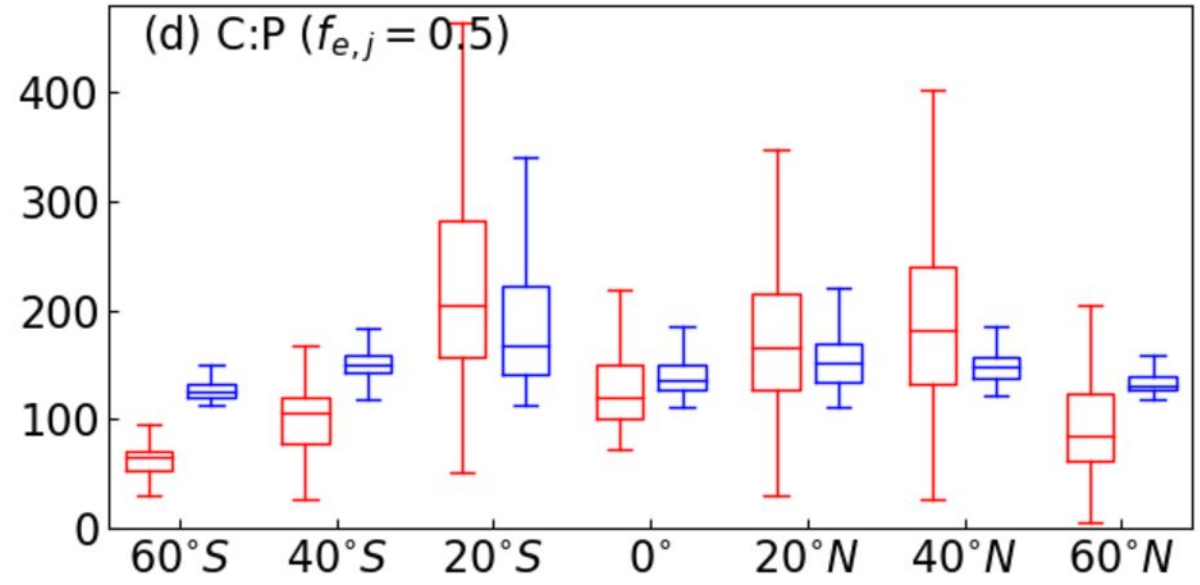

(b) C:N ($f_{e,j} = 0.7$)

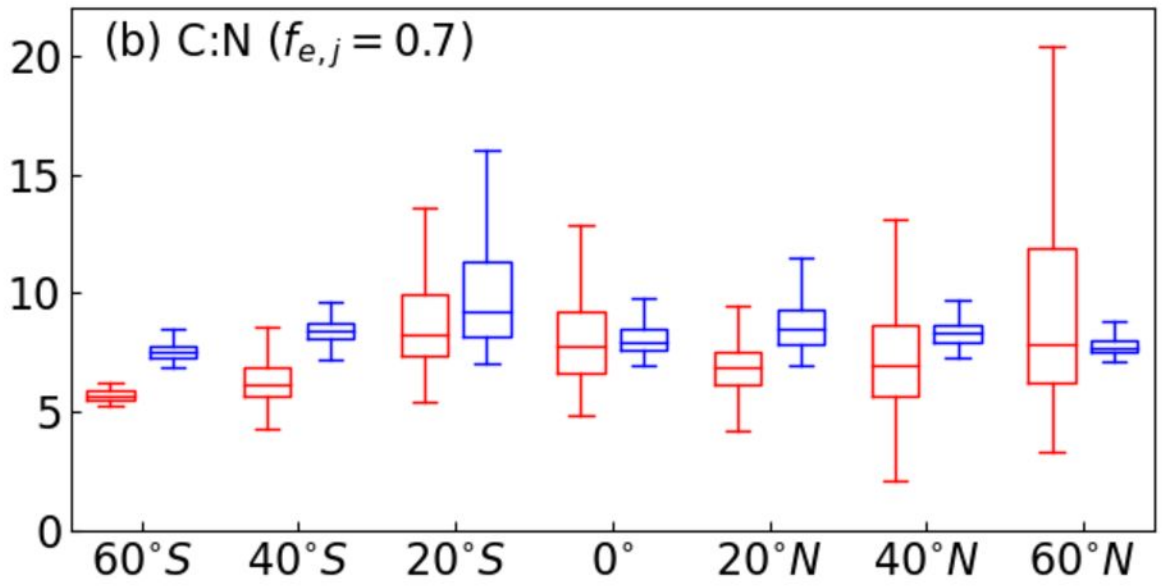

(e) C:P ($f_{e,j} = 0.7$)

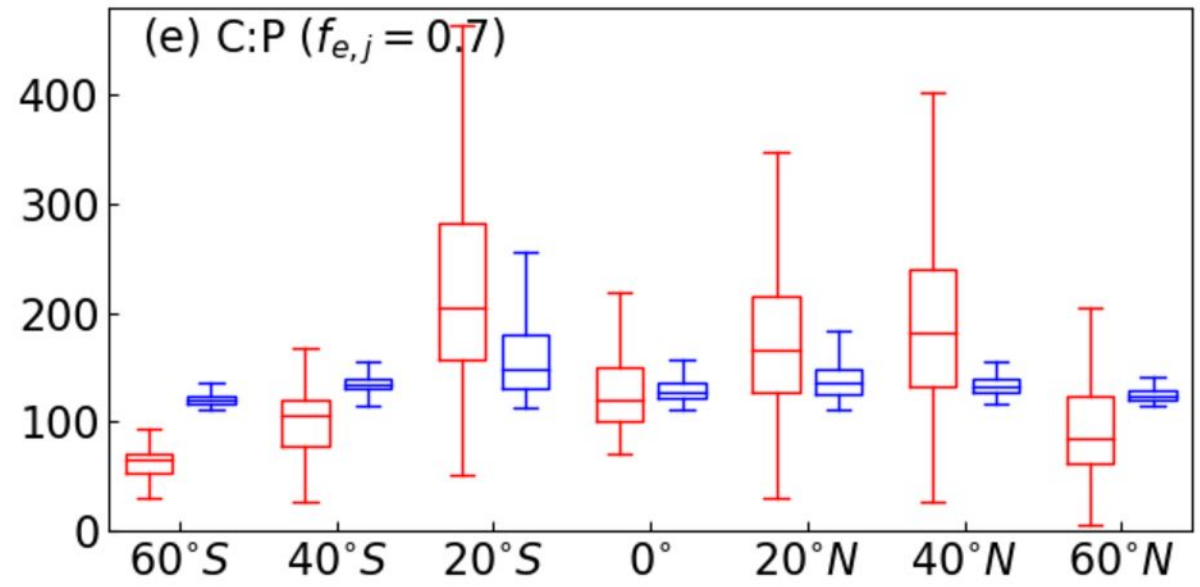

(c) C:N ($f_{e,j} = 0.9$)

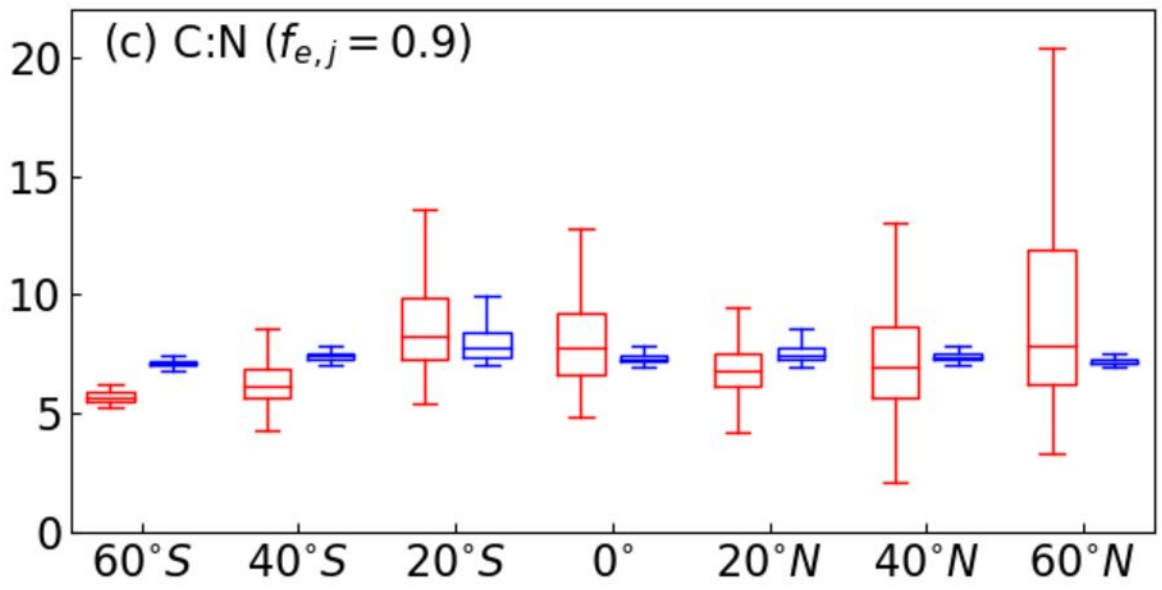

(f) C:P ($f_{e,j} = 0.9$)

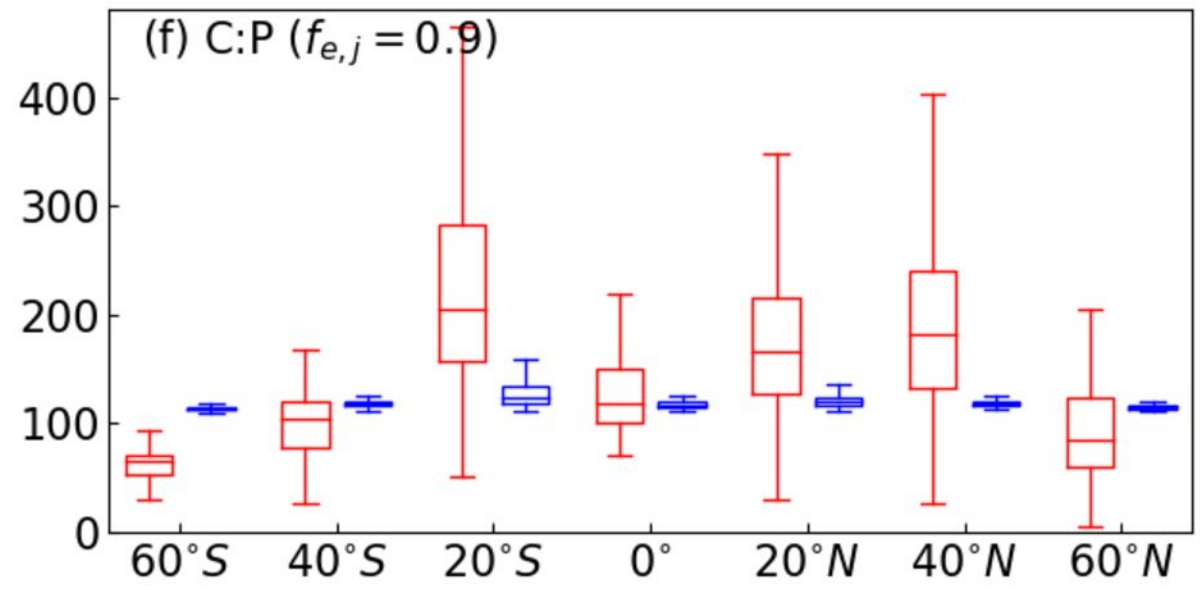

Figure 8.

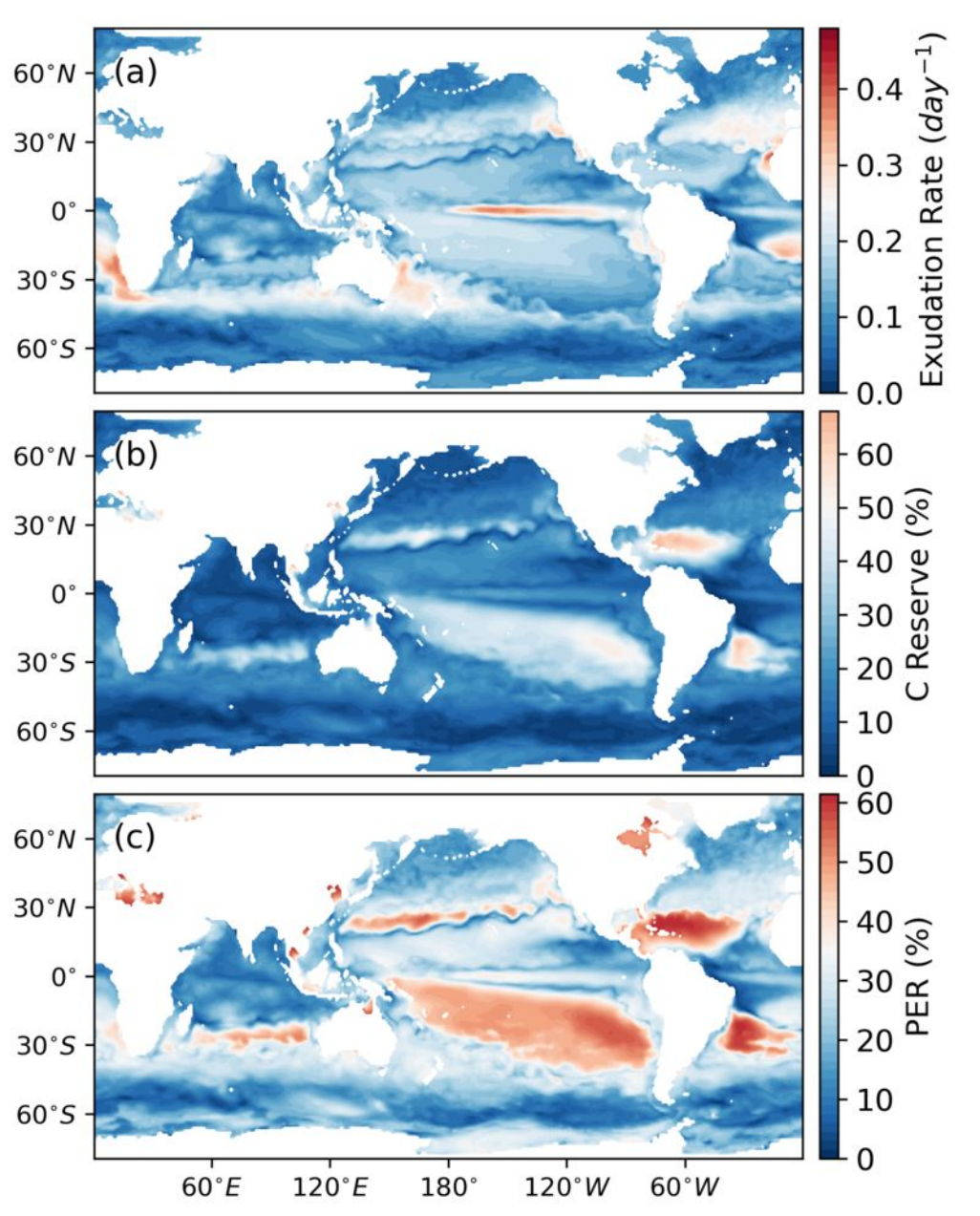
(a)
(b)
(c)
60°N
30°N
0°
30°S
60°S
60°E
120°E
180°
120°W
60°W
Exudation Rate (day^{-1})
0.0
0.1
0.2
0.3
0.4
C Reserve (%)
PER (%)
0
10
20
30
40
50
60